Modeling high burnup fuel thermochemistry, fission product release and fuel melting during the VERDON 1 and RT6 tests

A. Germain, J. Sercombe, C. Riglet-Martial, C. Introïni, L. Noirot, Y. Pontillon, Ph. Maugis, C. Guéneau

Modeling high burnup fuel thermochemistry, fission product release and fuel melting during the VERDON 1 and RT6 tests

A. Germain[a], J. Sercombe[a], C. Riglet-Martial[a], C. Introïni[a], L. Noirot[a], Y. Pontillon[a], Ph. Maugis[b] and C. Guéneau[c]

[a] CEA, DES, IRESNE, DEC, 13018 Saint-Paul-Lez-Durance, France
[b] Aix-Marseille University, CNRS, IM2NP, 13397 Marseille, France
[c] CEA, DES, IRESNE, DPC, 91191 Gif-sur-Yvette, France

Abstract

This paper presents simulations of the VERDON 1 and RT6 tests (temperature increase up to fuel-clad melting, oxidizing and/or reducing conditions within the furnace) performed with high burnup UO_2 fuel (i.e., up to 72 GWd/tU) and considering a coupling between irradiated fuel thermochemistry and a fission gas release model. The thermochemical calculations rely on the Thermodynamics of Advanced Fuels - International Database (TAF-ID) for the description of the phases likely to form from the 15 fission products considered in the fuel (Ba, Ce, Cs, I, La, Mo, Nd, Np, Pd, Rh, Ru, Sr, Tc, Te, Zr) and on the OpenCalphad solver for the minimization of the Gibbs energy of the system. The gas release model describes a diffusion process for the gases within equivalent spherical grains. It accounts for the gases formed by reaction between the fission products as well as the chemically inert noble gases. The progressive fission products depletion of the fuel due to their release in gas form closes the coupling. The impact of the fission products release kinetics on the thermochemical equilibria within the fuel is then studied by coupling the thermochemical calculations with a gas diffusion model. This approach is then extended to the RT6 test conditions (i.e., oxidizing). The coupled simulations led to a very good agreement with the release kinetics of various fission products (I, Te, Cs, Mo, Ba). The released fractions of the low-/non-volatile fission products and of uranium, plutonium are also well reproduced. The observed differences in the fuel-clad melting temperatures in the two tests (2200 °C during RT6 and 2600 °C during VERDON 1) are however not reproduced by the simulations.

1 Introduction

During severe accidents, fuel rod melting can occur together with significant Fission Product (FP) release. Past experimental programs have shown that the "collapse" of irradiated fuel rods (i.e., "fuel collapse" refers here to the loss of structural integrity of the fuel and cladding related to partial melting) can take place at temperatures far below the liquidus of fresh fuel ($\sim$ 2800 °C). See for instance Figure 16 of reference [1] where the collapse of fuel rods of high burnups between 47 and 70 GWd/tU during the VERCORS test series was observed at temperatures as low as 2100-2450 °C [2]. This behavior has several origins, ranging from the oxidizing conditions

taking place in the tests that lower the melting temperature of UO_2 [3] to the formation of a liquid phase in the fuel-cladding material when melting of the cladding has taken place and filled the fuel cracks [4][5]. The presence of FPs is also expected to lower to some extent the melting temperature of the fuel [6].

Simulation of fuel behavior during severe accidents up to fuel "collapse" can benefit from advanced thermochemical calculations that can deal with varying external conditions (oxidizing to reducing), clad melting, chemical reactions with FPs, clad zirconium liquefaction in uranium dioxide. As shown in a recent paper [7], the Thermodynamics of Advanced Fuels - International Database (TAF-ID [6]) is well suited for that purpose. Thermochemical equilibrium calculations of the VERDON 1 test with the TAF-ID have shown some consistency with the measured release of some FPs (Ba, Cs, Mo and Zr), i.e., the temperatures where significant FP release took place were consistent with the formation of gaseous compounds incorporating the released FPs. The formation of a mixed $(U,Zr)O_{2-x}$ liquid phase characterizing the melting of the fuel-cladding at a low temperature of ~ 2500 °C was also calculated, in good agreement with the post-VERDON 1 SE-SEM (Secondary Electron Scanning Electron Microscopy) observations [4].

Historically, most severe accident codes rely on simplified thermodynamic calculations, as detailed in a recent review of thermodynamically informed nuclear fuel codes [8]. Advanced thermodynamic calculations rely on the contrary on the Gibbs Energy Minimization (GEM) technique. One difficulty in the modeling of severe accident sequences with thermodynamic calculations based on a GEM is related to the necessary inclusion of fission gas release kinetics to properly assess the release of volatile, semi-volatile and low/non volatile FPs. In this respect, severe accident codes can include as much as three different transport mechanism to describe the release of the FPs [9][10][11][12][13][14]. The first one is generally related to the diffusion of the FPs in atomic form from the fuel grains to the grain boundaries. The second one describes the progressive release of the FPs from the grain boundaries and/or the pores of the fuel. When the fuel microstructure is not detailed in the codes, the second mechanism describes the transport of the semi-volatile FPs through a gaseous boundary layer located between the fuel surface and the bulk of the carrier gas [10][14]. The third one relates the release of the low-volatile FPs to fuel volatilization at high temperature. As can be infered, the consideration of three different gas transport mechanisms with advanced thermodynamic calculations relying on a GEM is not a straightforward matter.

In this paper, advanced thermochemical calculations of the VERDON 1 and VERCORS RT6 tests with the TAF-ID are coupled to a fission gas release model. The coupling strategy proposed by Germain et al. [15] between GEM calculations performed with another thermodynamic database (TBASE) and fission gas release kinetics is here extended to the TAF-ID to illustrate the versatility of this approach. The coupling strategy relies on a single diffusion mechanism accounting for the gases formed by chemical reactions between the FPs in the fuel in addition to the noble chemically inert gases. This facilitates the consideration of advanced thermodynamic calculations since the distinction between FP transport mechanisms is not anymore necessary. The fission gas model has been implemented in the fuel performance code ALCYONE of the PLEIADES computational environment [16][17]. The TAF-ID calculations are made with the OpenCalphad software [18][19], already available in ALCYONE [20]. Simulations of the RT6 and VERDON 1 tests on a sibling rodlet but in different test condi-

tions (oxidizing), are performed. The calculated releases of the volatile, semi-volatile, low/non volatile FPs and of actinides are then compared to on-line or post-test measurements when available. The melting temperatures estimated in the simulations of the RT6 and VERDON 1 tests are then discussed.

2 Brief summary of the RT6 and VERDON 1 tests

Details on the VERDON 1 and RT6 tests and post-test characterization of the samples can be found in references [1][4][21][22] and [2][23][24][25], respectively. Only the main features will be recalled hereafter. The RT6 and VERDON 1 samples consisted of small rodlets extracted from UO_2-M5 fuel rods (4.5 % ^{235}U) irradiated in the Gravelines reactor in France up to an average burnup of 72 GWd/tU. After fabrication and just before the tests, the rodlets have been re-irradiated at low power during a few days in the OSIRIS experimental reactor in order to re-create the short-lived FPs inventory. The RT6 and VERDON 1 rodlets contained respectively 3 and 2 pellets from the original fuel rod maintained between two depleted half pellets in the cladding tube clamped at both ends. The rodlets were heated in a furnace with permanent injection of a carrier gas composed of H_2/H_2O and He in order to control the atmosphere in contact with the fuel.

The temperature and carrier gas composition during the tests are presented in Figure 1. The VERDON 1 test was the first of a series following the closing of the VERCORS testing facility and was thus designed to check the behavior of the new facility. In this respect, the carrier gas composition during the first part of the VERDON 1 test was very similar to the one considered during the RT6 test.

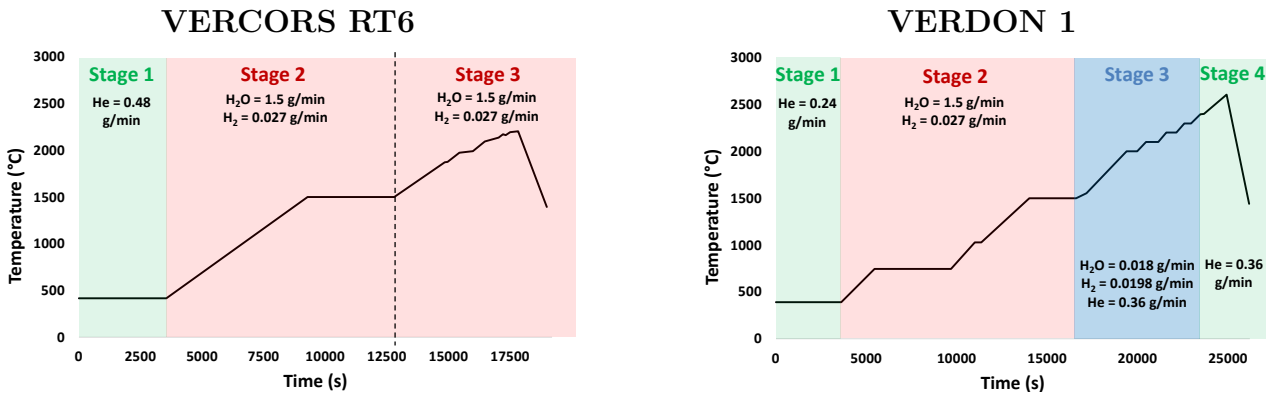

Figure 1: Temperature evolution and injected gas composition during the RT6 (left) and VERDON 1 (right) tests.

The experimental sequence began with a cold plateau at around 400 °C under an inert helium flow. The temperature was then progressively increased under an oxidizing atmosphere (high H_2O/H_2 ratio) and maintained at a final plateau of 1500 °C during 1 h to ensure the

full oxidation of the cladding (test part referred to as stage 2). On the contrary, the high temperature part of the RT6 (stage 3) and VERDON 1 tests (stage 3 and 4) differ since a reducing atmosphere was set in the furnace during the VERDON 1 test (low H_2O/H_2 ratio) while the same oxidizing conditions were kept during the RT6 test. In both tests, temperature was increased to 2200 °C for RT6 and 2400 °C for VERDON 1, respectively, with small plateaus at intermediate temperature levels. In the last part of the VERDON 1 test (stage 4), the carrier gas composition was switched back to helium due to a technical problem (shortage of H_2). The temperature increased up to $\sim$ 2600 °C before cooling down.

The measured fractions of xenon, iodine, tellurium, cesium, barium, molybdenum and zirconium released during the RT6 and VERDON 1 tests are plotted in Figure 2.

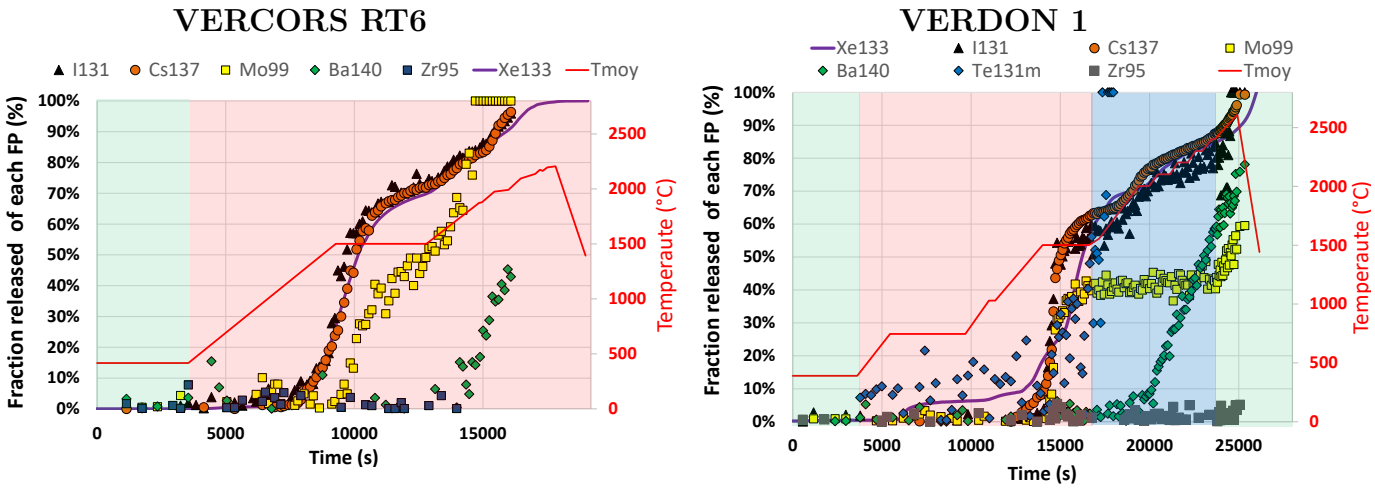

Figure 2: Fractions of Xe, I, Te, Cs, Ba, Mo and Zr released during the RT6 (left) and VERDON 1 (right) tests, as measured by online gamma spectrometry. Xe133 experimental release is plotted with a line to better show the resemblance with the release of I131, Cs137 and Te131m.

During stage 2, the release of the FPs in the two tests is very similar. Differences are observed for Mo and Ba during stage 3 due to the RT6 oxidizing / VERDON 1 reducing atmospheres. As classified in the previous VERCORS tests [23], the FPs released during the VERDON 1 test can be categorized in three groups: volatile FPs (xenon, iodine, cesium, tellurium) with close to 100 % release, semi-volatile FPs (barium, molybdenum) with 50 to 100 % release strongly influenced by the oxido-reducing conditions in the test and low-volatile/non-volatile FPs, illustrated here by zirconium. Melting of the fuel was reported in RT6 at 2200 °C, which explains why the test was stopped at a rather low temperature. No fuel "collapse" was recorded during the VERDON 1 test in spite of the 2610 °C reached by the fuel. However, post-irradiation examinations showed the initiation of fuel-clad melting near the fuel periphery [26].

3 Modeling of the RT6 and VERDON 1 test

3.1 Fuel thermochemistry

In this work, the modeling procedure of the VERDON 1 test presented by Geiger et al. [7] has been used. Geiger et al. performed thermochemical calculations with the commercial software ThermoCalc (TC) using the Thermodynamics of Advanced Fuel International Database [6] (TAF-ID V8 version from January 2018). The thermodynamic modeling of oxide fuels rests largely on the description of the fluorite (U,Pu)O_2 phase from Guéneau et al. [27], where, apart from major actinides, minor actinides and fission products may also occupy the cation sites, both at hypo- and hyperstoichiometric oxygen conditions (see the "(U, Zr)O_2" or C1_MO2 model of Table 1). The liquid phases are described using the partially ionic two sublattice liquid model [28]. Here, the first sublattice is occupied by cations, and the second by anions, "hypothetical vacancies" and neutral species. This allows for both purely metallic and ionic liquids to be simulated by the same model. In the TAF-ID V8, 206 binary and 72 ternary sub-systems are assessed. The ternary sub-systems of interest for this work are: Ba-Mo-O, Ba-O-U, Ba-O-Zr, Ce-O-U, Cs-Mo-O, Cs-O-U, Cs-O-Zr, Gd-O-U, La-O-U, Mo-O-U, Mo-Pd-Rh, Mo-Pd-Ru, Mo-Rh-Ru, Nd-O-U, O-Pu-U, O-Pu-Zr, O-Sr-U, O-Sr-Zr, O-U-Zr, Pd-Rh-Ru, Pu-U-Zr. The sublattice models for the phases discussed in the next sections of this paper are listed in Table 1. An extended description of the TAF-ID is given in reference [6].

Table 1: Composition of the phases encountered in the calculations. "Va" indicates a vacancy in the sublattice. In brackets, the name of the phases in the TAF-ID database.

Gas phase	(GAS)
	(Ba, Ba_2, BaH, BaI, BaI_2, BaO, Ba_2O, Ba_2O_2, $BaMoO_4$, BaOH, BaO_2H_2, Ce, CeO, Cs, Cs_2, CsH, CsI, Cs_2I_2, Cs_2MoO_4, CsO, Cs_2O, Cs_2O_2, CsTe, Cs_2Te, Cs_2Te_2, Cs_2Te_3, Gd, GdO, H, H_2, HI, HO, HO_2, H_2O, H_2O_2, HTe, H_2Te, HIO, He, I, I_2, La, LaI_3, LaO, LaO_2, La_2O, La_2O_2, LaTe, Mo, Mo_2, MoI, MoI_2, MoI_3, MoI_4, MoO, MoO_2, MoO_3, Mo_2O_6, Mo_3O_9, Mo_4O_{12}, Mo_5O_{15}, MoO_2I_2 Nd, NdO, Np, NpO, NpO_2, O, O_2, O_3, Pd, Pu, PuO, PuO_2, Rh, RhO, RhO_2, Ru, RuO, RuO_2, RuO_3, RuO_4, RuO_2H_2, Sr, Sr_2, SrH, SrI, SrI_2, SrO, SrOH, SrO_2H_2, Te, Te_2, Te_3, Te_4, Te_5, Te_6, Te_7, TeI_2, TeI_4, TeO, TeO_2, Te_2O_2, U, UI, UI_2, UI_3, UI_4, UO, UO_2, UO_3, Zr, Zr_2, ZrH, ZrI, ZrI_2, ZrI_3, ZrI_4, ZrO, ZrO_2)
$(U,Zr)O_2$	Fluorite phase (C1_MO2)
	$(Ce^{3+}, Ce^{4+}, Gd^{3+}, La^{3+}, Nd^{3+}, Np^{3+}, Np^{4+}, Pu^{3+}, Pu^{4+}, U^{3+}, U^{4+}, U^{5+}, Zr^{2+}, Zr^{4+})_1$ $(O^{2-}, Va)_2$ $(O^{2-}, Va)_1$
$BaZrO_3$	Perovskite phase (PEROVSKITE)
	$(Ba^{2+}, Sr^{2+})_1$ $(Ba^{2+}, U^{4+}, Mo^{4+}, U^{6+}, Zr^{4+})_1$ $(O^{2-})_3$
ZrO_2-M	Monoclinic zirconia phase (ZRO2_MONO)
	$(Zr^{4+})_1$ $(O^{2-}, Va)_2$
ZrO_2-T	Tetragonal zirconia phase (ZRO2_TETR)
	$(Ba^{2+}, U^{4+}, Zr^{4+})_1$ $(O^{2-}, Va)_2$
Liquid	Liquid phase (LIQUID)
	$(Ba^{2+}, Ce^{3+}, Cs^{+}, Gd^{3+}, La^{3+}, Mo^{4+}, Nd^{3+}, Np^{4+}, Pd^{2+}, Pu^{3+}, Rh^{3+}, Ru^{4+}, Sr^{2+}, Tc^{4+}, U^{4+}, Zr^{4+})_P$ $(I^{-}, MoO_4^{2-}, O^{2-}, Va^{Q-}, CeO_2, CsO_2, Cs_2Te, I_2, MoO_3, O, Te, PuO_2, TeO_2)_Q$
FCC	Face Centered Cubic metallic phase (FCC)
	(Ba, Ce, Cs, Gd, La, Mo, Pd, Pu, Rh, Ru, Tc, Te, U, Zr)$_1$ (O, Te, Va)$_1$
HCP	Hexagonal Close Packed metallic phase (HCP)
	(Ba, Ce, Cs, Gd, Mo, Pd, Pu, Rh, Ru, Tc, U, Zr)$_1$ (O, Va)$_{0.5}$
	Stoichiometric phases
$BaMoO_4$	$BaMoO_4$
CsI	CsI
Cs_2MoO_4-O	Cs_2MoO_4
Cs_2MoO_4-H	Cs_2MoO_4
MoO_2	MoO_2
MoO_3	MoO_3
MoRh	MoRh
$MoRh_3$	$MoRh_3$

The initial FP inventory was estimated by Geiger et al. from neutronics calculations with the CESAR code [29] performed on a MOX U-Pu-O fuel with 4.5 wt% Pu reaching an average burnup of 60 GWd/tHM. To match the burnup and the inital composition of the VERDON 1 sample, Geiger et al. linearly extrapolated the FP content to an average burnup of 72 GWd/tHM. This approach obviously leads to some approximation in the FP inventory but was

kept for the sake of comparison to the calculations of Geiger et al. Also the aim of this paper is not to discuss in details the initial FP inventory in the fuel but to show that a single gas diffusion mechanism for the gas phase coupled to thermochemistry can lead to consistent FP release predictions. Fifteen representative FP elements were used by Geiger et al. [7] in the TAF-ID calculations to represent the wide spectrum of FPs available in irradiated fuel: Ba, Ce, Cs (Cs+Rb), I (I+Br), La (La+Y), Gd (Gd+Tb+Dy+Ho), Mo, Nd (Nd+Pm+Sm+Eu), Pd (Pd+Ag+Cd+In+Sn+Sb), Rh, Ru, Sr, Tc, Te (Te+Se+Ge+As), Zr (Zr+Nb) together with the U, O, Pu (Pu+Am+Cm) and Np content of the irradiated pellets. The U, O content of the two depleted half-pellets and the Zr content of the cladding were also included in the thermochemical calculations. The carrier gas injected during each stage of the test was also added in the simulations.

The calculation of the VERDON 1 test was performed by dividing the test in four main parts (called "stage") related to changes in the carrier gas composition. During each stage, the same elemental composition (which included all the Zr from the cladding) was used in the thermochemical calculations assuming a constant pressure of 1 bar. Only the temperature was changed to follow the test sequence. Stage 1 was not calculated since the low temperature reached was not expected to lead to significant changes in the fuel phase composition. The elemental mole numbers used by Geiger et al. [7] in the different stages are recalled in Figure 3. The following strategy was considered by Geiger et al. to account for the fission products released at the end of each stage. The moles of FPs that were found in the gas phase at the end of each stage were removed from the elemental mole numbers used at the next stage. This is the reason why the mass of iodine, cesium and tellurium are equal or very close to 0 mol during stage 3.

Stage 2	
Duration (s)	16522
Atmosphere	
H2 (g)	7.435
H2O (g)	413.05
System Composition	
Element	moles
Ba	1.53E-04
Ce	2.49E-04
Cs	2.91E-04
Gd	1.36E-05
I	2.33E-05
La	1.20E-04
Mo	4.79E-04
Nd	3.71E-04
Np	2.38E-05
O (Fuel)	1.64E-01
Pd	1.92E-04
Pu	3.55E-04
Rh	5.45E-05
Ru	3.32E-04
Sr	1.30E-04
Tc	1.10E-04
Te	5.25E-05
U	5.25E-02
Zr (cladding)	7.64E-02
Zr (FP)	5.28E-04

Stage 3	
Duration (s)	6842
Atmosphere	
H2 (g)	2.258
H2O (g)	2.053
System Composition	
Element	moles
Ba	1.48E-04
Ce	2.49E-04
Cs	0
Gd	1.36E-05
I	0
La	1.20E-04
Mo	9.61E-05
Nd	3.71E-04
Np	2.38E-05
O (Fuel)	2.62E-01
Pd	1.10E-04
Pu	3.55E-04
Rh	5.45E-05
Ru	3.32E-04
Sr	1.30E-04
Tc	1.10E-04
Te	0
U	5.25E-02
Zr	7.69E-02

Stage 4	
Duration (s)	1362
Atmosphere	
He (g)	8.172
System Composition	
Element	moles
Ba	6.10E-06
Ce	2.48E-04
Cs	0
Gd	1.36E-05
I	0
La	8.44E-05
Mo	8.20E-05
Nd	3.71E-04
Np	2.38E-05
O (Fuel)	2.58E-01
Pd	0
Pu	3.55E-04
Rh	2.55E-05
Ru	3.15E-04
Sr	1.25E-04
Tc	1.10E-04
Te	0
U	5.17E-02
Zr	7.69E-02

Figure 3: Input parameters used in the thermochemical equilibrium calculations [7].

In the simulations of this work, the thermochemical solver OpenCalphad (OC) was used with the same thermodynamic database TAF-ID V8. All the results obtained by Geiger et al. [7] concerning the chemical speciation of I, Te, Cs, Mo, Ba, Zr in the fuel-cladding during the VERDON 1 test were reproduced. This includes in particular the melting of the (U,Zr)O_{2-x} phase (uranium dioxide dissolved in the clad zirconium) between 2500 and 2600 °C, supported by numerous post-test examinations [4]. This calculation leads also to an interesting gas phase composition evolution during the VERDON 1 test. A synthesis of the calculated proportion of each FP in the gas phase during the VERDON 1 test is proposed in Figure 4. This graph can be compared to Figure 14 of reference [7].

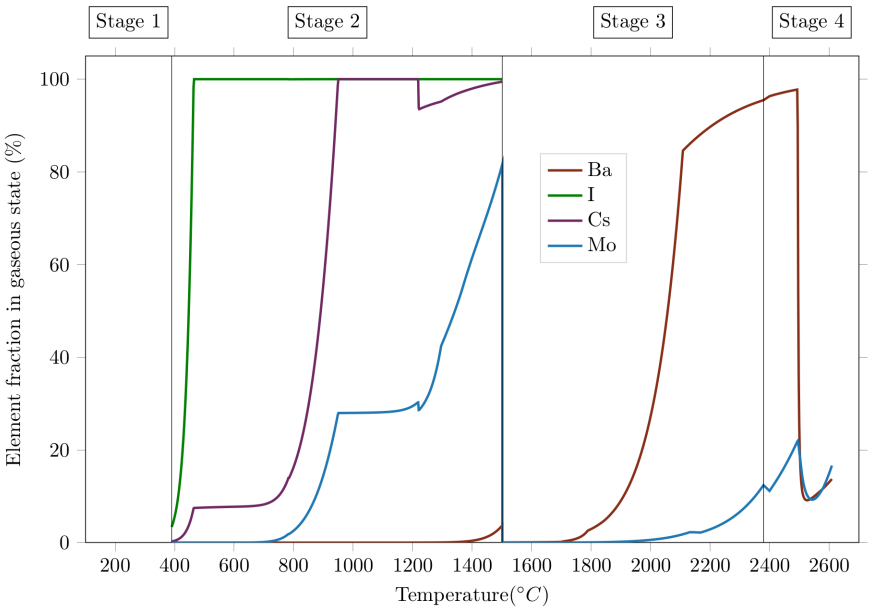

Figure 4: Predicted percentage of each FP in the gas phase during the VERDON 1 test, as a function of temperature. Calculations made with OC following the methodology of Geiger et al. [7].

The predicted behavior of the volatile FPs (I, Te and Cs) is characterized by a 100 % proportion in the gas phase at the end of stage 2. Seventy to eighty percent of molybdenum is found in the gas phase at the end of stage 2. During stage 3 (reducing conditions), molybdenum is only slightly available in the gas phase which is consistent with the measured stable released fraction (see Figure 2). During stage 4, the proportion of Mo in the gas phase increases again as the measured released fraction. Barium appears in the gas phase at around 1700 °C and its proportion increases to reach 100 % at the end of stage 3. This is consistent with the progressive release that was measured at the same period during the VERDON 1 test and that led to a final released fraction of Barium of 72 %, see Figure 2.

3.2 Fission gas diffusion

The calculations performed by Geiger et al. with the TAF-ID did not include fission gas release. Results could therefore not be compared directly to on-line FP release rates. Fission gas release kinetics is of crucial importance for volatile FPs such as I and Cs since a proportion of 100 % is found in the gas phase at temperatures below 1000 °C. This is obviously inconsistent with their progressive release during the RT6 and VERDON 1 tests. On the contrary, the proportion of the semi-volatile FPs Mo and Ba in the gas phase during the different stages of the VERDON 1 simulation, as shown in Figure 4, is globally consistent with the periods where these FPs are released during the test (Figure 2). As an example, the proportion of Mo in the gas phase is very small during stage 3 which is consistent with the non significant release of Mo. These results support the idea that the release of semi-volatile FPs in these experimental conditions is mostly

thermodynamically controlled. Therefore, a coupling of these thermochemical calculations with a fission gas release model should lead to some agreement with the measured on-line FP release.

Recently, a coupling strategy between fuel thermochemistry and fission gas release that can be incorporated in fuel performance codes was proposed by Germain et al. [15]. In this approach, fission gas release is described by a simple diffusion model in an equivalent spherical fuel grain considering the bulk of the gas phase with no distinction between the FPs:

$$\frac{\partial C}{\partial t} = \frac{1}{r^2}\frac{\partial}{\partial r}\left(Dr^2\frac{\partial C}{\partial r}\right) + \frac{\partial S_{FP}}{\partial t} \tag{1}$$

where C is the total gas concentration (in mole/m^3), D is the effective diffusion coefficient (in m^2/s) and r is the radial position in the sphere (in m). The specificity here is the inclusion of the term $\partial S_{FP}/\partial t$ (in mole/m^3/s) related to the gases formed from chemically reactive FPs, as calculated from the thermochemical equilibria. The boundary condition at the spherical grain surface is $C(r = a, t) = 0$ with a the grain radius in m and t the time in s. Instantaneous release of the gas from the fuel is thus assumed when it reaches the grain surface. The diffusion coefficient D is given by the following expression:

$$D(T) = D_0 \exp\left(-\frac{Q}{RT}\right) \tag{2}$$

with Q representing the activation energy (in J/mol) and D_0 a constant parameter (in m^2/s). R is the ideal gas constant (in J/mol/K) and T the temperature in K. The abundant and inert FP Xe generally represents the bulk of the gas phase in the fuel and can be used as an indicator of the release rate of all the gases from the fuel. The model parameters can therefore be fitted on the measured release kinetics of Xe. In medium burnup fuel ($\sim$ 40 GWd/tU), equations 1 and 2 lead to a reasonably good estimation of the release of Xe during the VERCORS 4 and 5 tests [15]. Modeling fission gas release during the RT6 and the VERDON 1 tests on a high burnup fuel with the same approach is more difficult since the measured release kinetics of Xe are characterized by several peaks of varying magnitude, as shown in Figure 5.

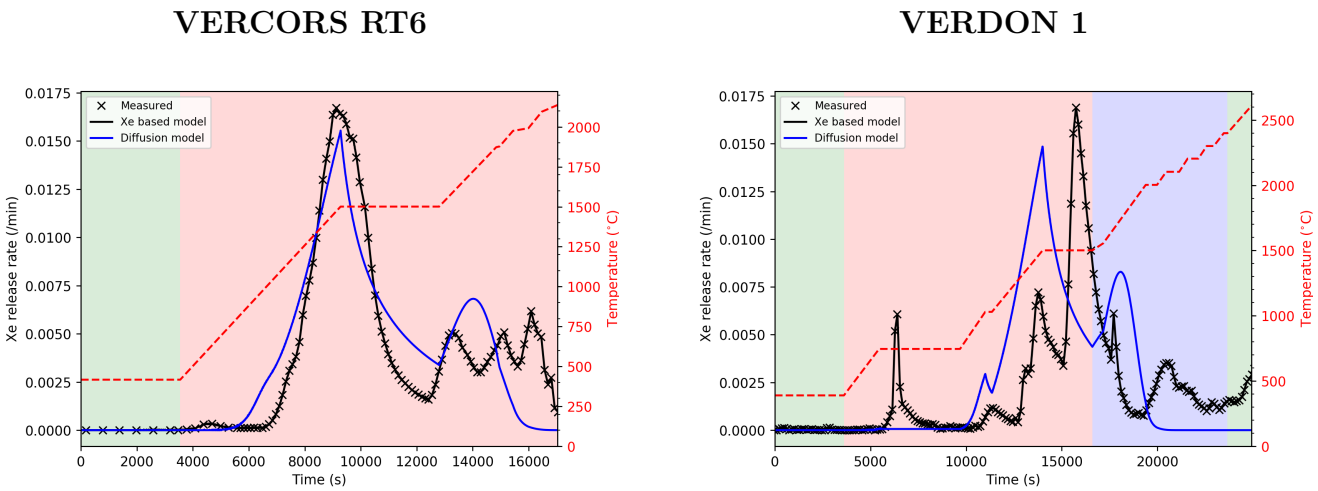

Figure 5: Measured and fitted release rate of ^{133}Xe during the RT6 (left) and VERDON 1 (right) tests.

The fitting of the Xe release rate indicated by the blue lines in Figure 5 relies on a single parameter, $D_0 = 2.17 \times 10^{-10}$ m^2/s. The activation energy $Q = 188$ kJ/mol is the one identified by Booth [30]. While the fit can be considered fair for RT6, it is far from the complex Xe release rate measured during VERDON 1. The numerous burst releases at low temperature are impossible to catch. The calculated main peak during the VERDON 1 test takes place too soon compared to the measurements. It is inferred that a proper estimation of the fission gas distribution before the test, whether dissolved in the grains, or within bubbles in the grains or at the grain boundaries, is necessary to better model the release of Xe. It is out of the scope of the present paper to propose a detailed description of fission gas distribution within irradiated fuel. This aspect is usually treated by dedicated models in fuel performance codes [12],[10], but is usually restricted to noble and chemically non-reactive gases. Nevertheless, to study the impact of the Xe release rate fitting on the release of the other FPs, the measured Xe release rate has also been used directly in the coupled model and results compared to those of the diffusion model. The black lines of Figure 5 represent the fitted release rates with respect to the initial quantity of Xe (refered as "Xe based model" in the rest of the paper). The experimental points are interpolated when necessary to allow a calculation with a 10 s time step.

3.3 Coupling thermochemistry with fission gas release

The coupling strategy relies on a time discretization of the tests with thermochemical equilibrium calculations and fission gas release evaluations at each time step. The fission gas release calculation is based on the numerical solution of equation 1 or on the direct use of the measured Xe release rate. In the first case, a thermochemical equilibrium calculation is performed before solving equation 1 in order to define the amount of FPs in the gas phase and therefore the source term $\partial S_{FP}/\partial t$ (in mole/m^3/s). Equation 1 is solved at each time step by the finite volume method leading an estimation of the gas flux J (in mole/m^2/s) at the grain boundary:

$$J = -D \left. \frac{\partial C}{\partial r} \right|_{r=a} \tag{3}$$

The FP inventory is then updated to account for the progressive release of the gas species found in the fuel. The release rate RR (in mole/s) at each time step of a FP indexed i is thus obtained from the following expression:

$$RR(FP_i) = \frac{\int_S J dS}{\int_V C dV} \times \int_V c_{FP_i} dV \tag{4}$$

where $\int_V c_{FP_i} dV$ (in mole) is the FP i content in the gas phase in the grain (from thermochemistry), $\int_V C dV$ is the total gas content in the grain (in mole), V the grain volume (in m^3) and S the surface of the grain (in m^2). Dividing RR by the initial content in FP i and multiplying by the time step produces the fraction of FP_i released during the time step. The sum of these instantaneous release fractions can be directly compared to on-line measurements shown in Figure 2. As an alternative to solving equation 1, and since noble gases represent the bulk of the gas phase, the measured Xe release rate can be used to define the instantaneous release rate R. In this case, the contribution of reactive FPs is not considered ($\partial S_{FP}/\partial t = 0$). With this coupled approach, the impact of the progressive depletion in FPs on the thermochemical calculations can here be studied in details and FPs release rates assessed.

In the TAF-ID calculations of Geiger et al. [7], the entire carrier gas (H_2O, H_2 and/or He) incoming in the furnace during a stage (i.e. flow rate $\times$ duration on the whole stage) is used as input at each temperature step (or each time step) of the calculation. Obviously, these calculation conditions are not representative of the actual test conditions as given in reference [15]. Since the gas circulates at a constant flow rate in the furnace, the amount of gas interacting with the fuel at each time step dt is actually equal to (flow rate $\times dt$) and not (flow rate $\times$ duration of the whole stage). In addition, that quantity of incoming gas is renewed at each time step in order to simulate the continuous circulation of the fresh gas in the furnace. In fact, as compared to the actual experimental conditions, those adopted by Geiger et al. [7] keep the same partial pressures of each species of the incoming gas (H_2O, H_2 and He), but the volume of gas interacting with the fuel at each step of temperature (or time) is not respected. In consistency with the actual test conditions (as considered in reference [15]), the coupling strategy employed in the present study considers only the amount of gas H_2O / H_2 / He interacting with the solid during the time step, that quantity being renewed at each time step. However, for the sake of comparison with the study of reference [7] using the same version of the TAF-ID, an additional fixed quantity of non-chemically reactive He is added in the simulation of the carrier gas in order to be consistent with the total amount of gas considered by Geiger et al. [7]. In the present calculation conditions, the same total amount of carrier gas and the same ratio of $p_{H_2O}/p_{H_2} \approx p_{O_2}$ is thus maintained as compared to Geiger's conditions, though the H_2O and H_2 partial pressures are somewhat different. It has been checked that this leads to thermochemical results in agreement with those given in reference [7]. As already specified, this evidently leads to an overestimation of the gas phase in interaction with the solid as compared to the actual test conditions. However, this calculation procedure has been kept here since the aim of the paper is not to discuss in details the thermodynamic modeling

included in the TAF-ID but to show that a single gas diffusion mechanism for the gas phase coupled to thermochemistry can lead to consistent FP release predictions. The impact of this overestimated gas phase on the FP chemical speciation will however be discussed in the course of the paper when necessary. The initial FPs inventory in the coupled model is given in Figure 3, stage 2. The same inventory is considered in the VERCORS RT6 and VERDON-1 simulations.

3.4 Fission product release and speciation predictions

3.4.1 Relative oxygen potential

The differences between the RT6 and VERDON 1 tests can first be highlighted by the plot of the relative oxygen potential defined by $\Delta G_{O_2} = RT \times \ln p_{O_2}$. ΔG_{O_2} is equal to the difference between the chemical potential of oxygen in the solid and that of pure gaseous oxygen at the same temperature and at 1 bar pressure [31].

The calculated evolution of this quantity during the two tests is given in Figure 6. For convenience, the plot is proposed as a function of temperature.

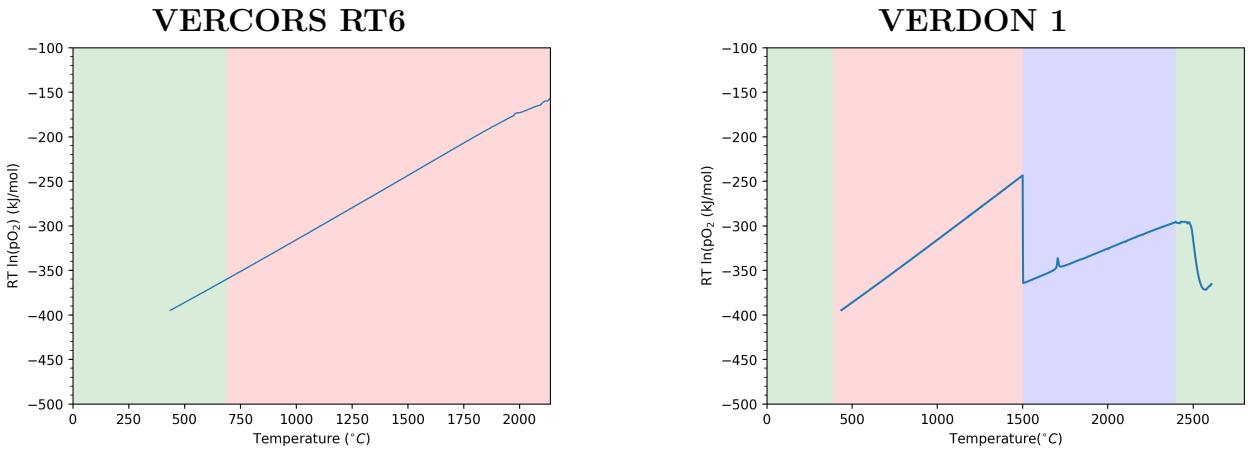

Figure 6: Calculated evolution of the relative oxygen potential as a function of temperature during the RT6 (left) and VERDON1 (right) tests.

During stage 2, the relative oxygen potential is the same in the two tests, being driven by the H_2O/H_2 ratio and the increasing temperature (up to 1500 °C). A step is observed at the interface between stages 2 and 3 during the VERDON 1 test due to the change in the carrier gas composition (i.e., oxidizing to reducing atmosphere). It is not the case during the RT6 test since the same carrier gas composition has been kept throughout the experiment. During stage 4 in the VERDON 1 test, the switch to a helium carrier gas with no chemical interactions with the fuel provides a situation where the relative oxygen potential is controlled by the reactions within the sample rather than by the external atmosphere. The quasi-constant oxygen potential close to -340 kJ/mol followed by a sharp decrease at 2550-2600 °C is a consequence of a solid-liquid transition in the $(U,Zr)O_2$ phase, as detailed in Geiger et al. [7]. At the end of the RT6

test (2200 °C), the relative oxygen potential is 100 kJ/mol higher than in the VERDON 1 test at the same temperature.

3.4.2 Iodine and tellurium

The calculated fractions of iodine and tellurium released during the RT6 and the VERDON 1 tests are compared in Figure 7 to on-line measurements. Note that Te was not measured during the VERDON 1 test.

The high availability of iodine and tellurium in the gas phase leads to an excellent agreement with the measured fractions released during the RT6 and VERDON 1 tests, especially when the Xe based model is used. The diffusion model leads to good results for RT6 but to an overestimation of iodine release kinetics during VERDON 1, as expected from the poor quality of the fit on the Xe release rate.

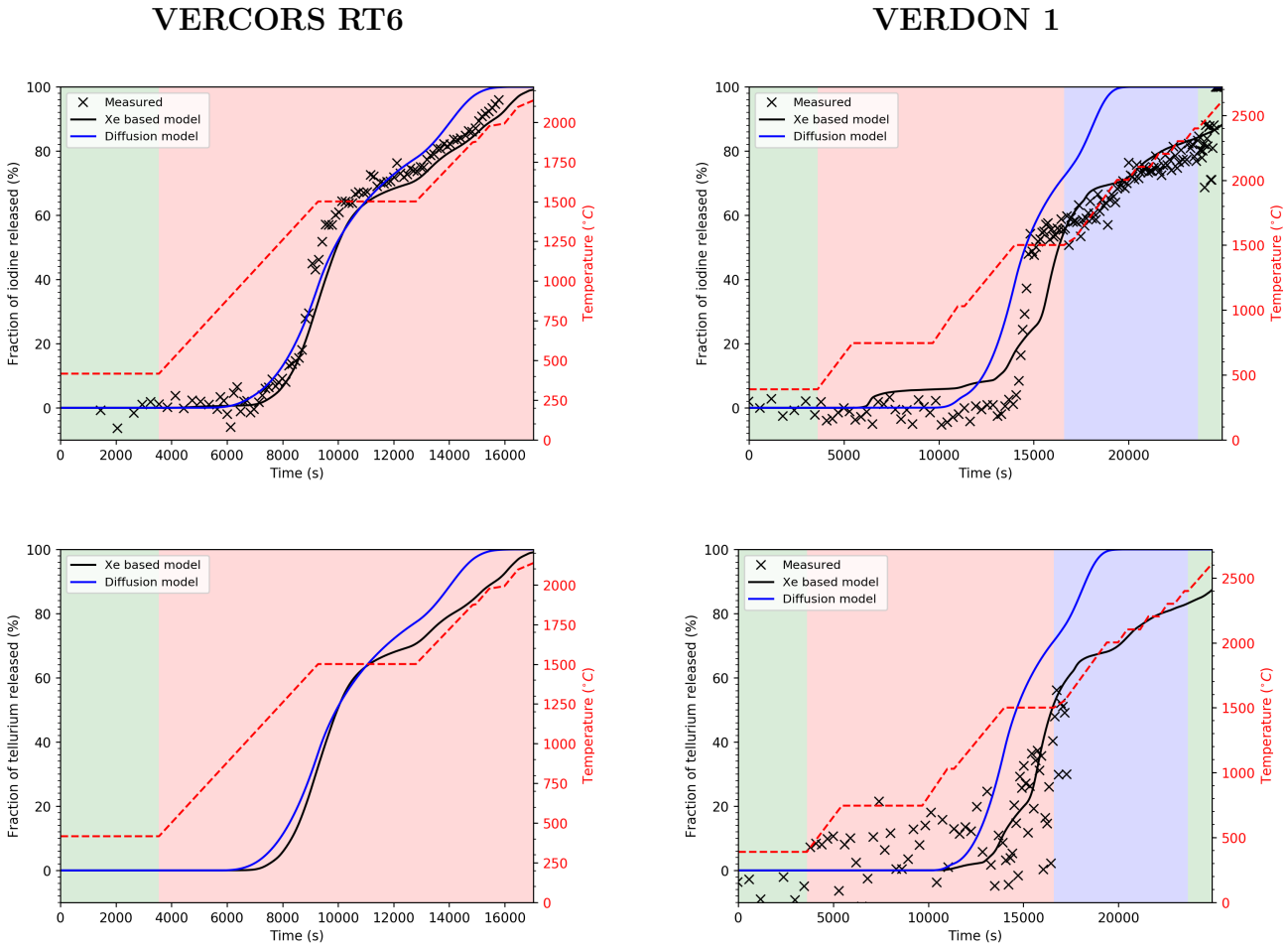

Figure 7: Calculated and measured fractions of iodine (top) and tellurium (bottom) released during the RT6 (left) and VERDON 1 (right) tests.

The calculated chemical speciations of iodine and tellurium in the gas phase during the RT6

test are illustrated in Figure 8 as a function of temperature.

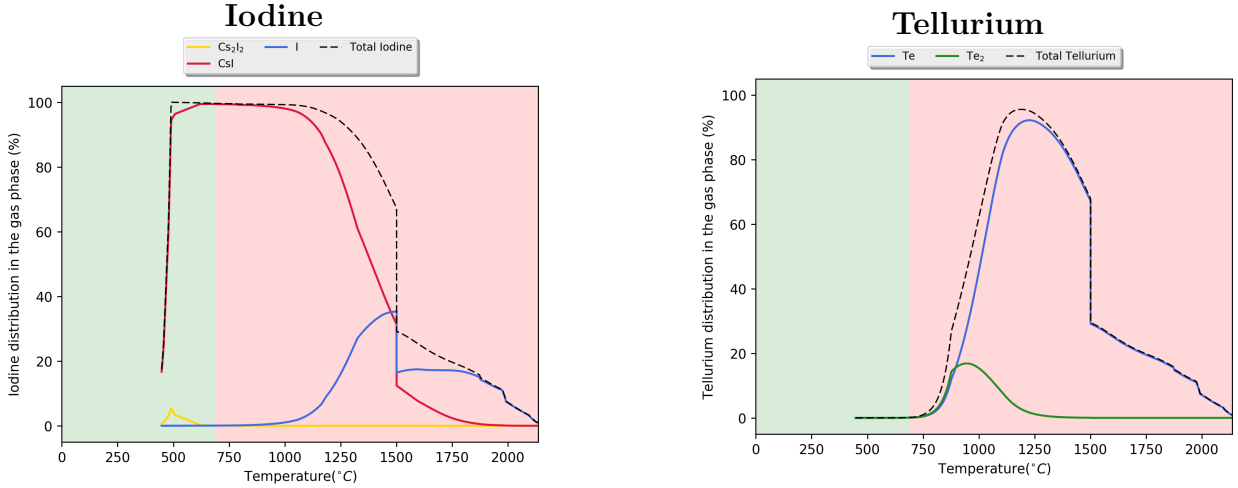

Figure 8: Chemical speciation of iodine (left) and tellurium (right) in the gas phase during the RT6 test as a function of temperature. Calculations made with the Xe based model.

These graphs confirm the high availability of the FPs iodine and tellurium in the gas phase. Tellurium speciation in the gas phase appears to be independent of the other FPs. Formation of atomic and diatomic tellurium occurs at 750 °C. One hundred percent of the tellurium in the fuel is found in the gas phase at 1200 °C. Seventy percent is released during the 1500 °C oxidation plateau. The remaining thirty percent is released during stage 3 where monoatomic tellurium is the main gaseous compound. The very stable species of tellurium in the gas phase are both independent of oxido-reduction and unreactive towards the other FPs. Therefore, from a chemical point of view, tellurium acts as a rare gas in severe accident tests, which explains why its behavior is usually consistent with that of Xe.

On the contrary, the speciation of iodine is not independent of the other FPs. Cesium iodide and for a smaller part Cs_2I_2 appear above 500 °C and incorporate 100 % of the iodine available in the fuel. At around 1000 °C, dissociation of cesium iodide starts in favor of atomic iodine. Iodine release is particularly important during the 1500 °C oxidation plateau, reaching 70 %. During stage 3, the chemical speciation remains the same leading to 100 % release at the end of the test. The chemical speciation of iodine and tellurium are very similar during the RT6 and VERDON 1 tests. In fact, the speciation of iodine and tellurium being independent of oxido-reduction in the test conditions, the behavior of those FPs is logically similar in both tests, in consistency with experimental observations.

3.4.3 Cesium

The calculated fractions of cesium released during the RT6 and VERDON 1 tests are compared in Figure 9 to on-line measurements. As for iodine and tellurium, the agreement with the measurements is really good, especially with the Xe based model. The Cs release during the VERDON 1 test is overestimated with the diffusion model.

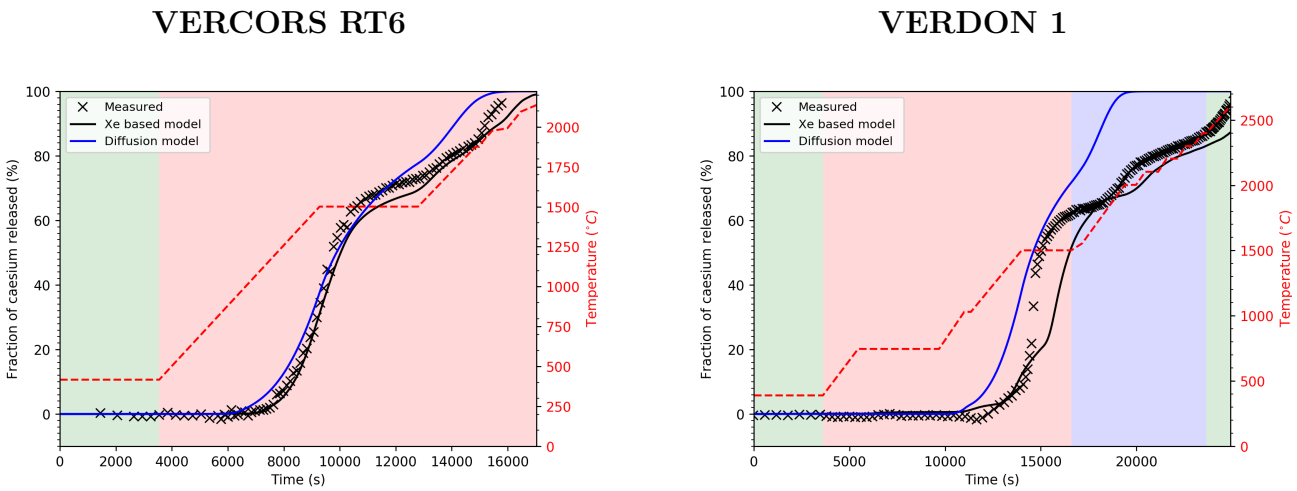

Figure 9: Calculated and measured fractions of cesium released during the RT6 (left) and VERDON 1 (right) tests.

The calculated chemical speciations of cesium in the gas phase during the RT6 and VERDON 1 tests are given in Figure 10 as a function of temperature.

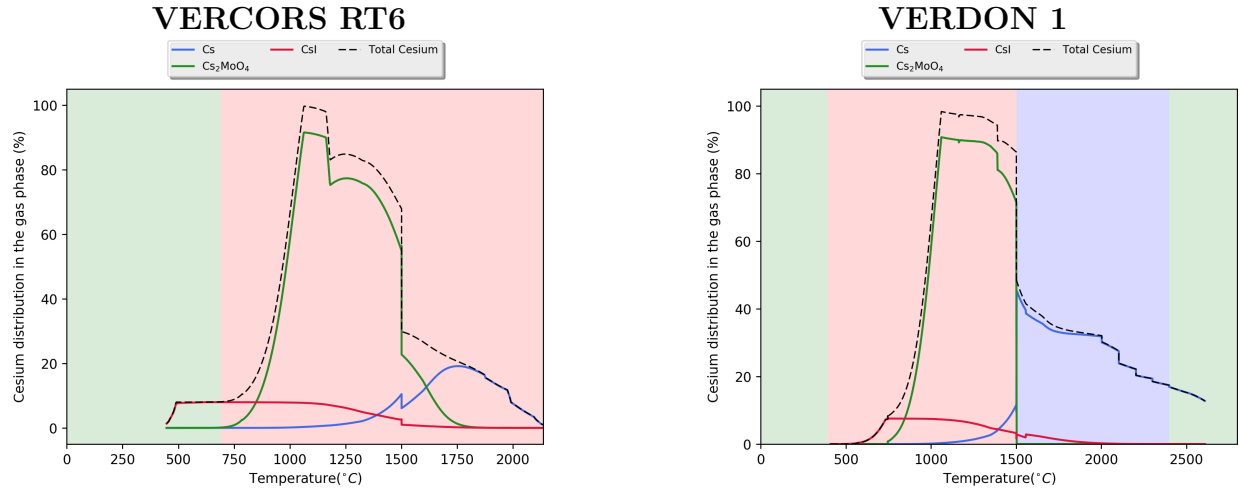

Figure 10: Chemical speciation of cesium in the gas phase during the RT6 (left) and VERDON 1 tests as a function of temperature. Calculations were performed with the Xe based model.

The chemical speciation of cesium in the gas phase is more complex than that of iodine and tellurium since it interacts with two other FPs, namely iodine and molybdenum. Vaporization of around 1/10th of cesium occurs above 500 °C leading to cesium iodide in quantity limited by the availability of iodine. At 700 °C, formation of cesium molybdate starts and increases with temperature until 90 % of cesium is incorporated. At 1050 °C, all cesium is in the gas phase. Small differences are visible in the RT6 and VERDON 1 simulations before the oxidation plateau is reached as a consequence of differences in the release rates. A sudden drop of the Cs

quantity in the gas phase occurs during RT6 at 1200 °C with the formation of a liquid phase that evaporates progressively with temperature increase. Simultaneously, atomic Cs appears in the gas phase and increases with temperature. 30 % (15 %) of cesium is released before the oxidation plateau in the RT6 (VERDON 1) test. Around 70 % (50 %) of cesium is released during the plateau in consequence of gas diffusion. The simultaneous release of iodine leads to a decrease of the quantity of cesium iodide in the fuel. During stage 3 of the RT6 test (oxidizing conditions), the same chemical speciation holds with Cs_2MoO_4 and Cs, leading to 100 % release at the end of the test. During the VERDON 1 test, the change to reducing conditions suppresses Cs_2MoO_4 from the gas phase in favor of gaseous Cs, according to the reaction $Cs_2MoO_{4(g)} + 4H_2 \rightleftarrows 2Cs_{(g)} + Mo_{(s)} + 4H_2O$.

3.4.4 Molybdenum and barium

The calculated fractions of molybdenum and barium released during the RT6 and VERDON 1 tests are compared in Figure 11 to on-line measurements. The agreement with the measured fractions of molybdenum released during the RT6 and VERDON 1 test is extremely good. The diffusion model performs nearly as well as the Xe based model because the release rate for this FP is more dependent on thermochemistry. The release in 3 steps (fast, slow, moderate) in both tests is well captured. The calculated barium release rate (thin black line) is also well reproduced with the Xe based model and begins almost at the same time than measured. The agreement is also good with the diffusion model in the case of RT6. The calculation for the VERDON 1 test with the same model leads to an overestimation of the Ba release rate, which is due to the poor fit of the Xe release rate where a peak is obtained around 1700 °C when Ba is found in the gas phase.

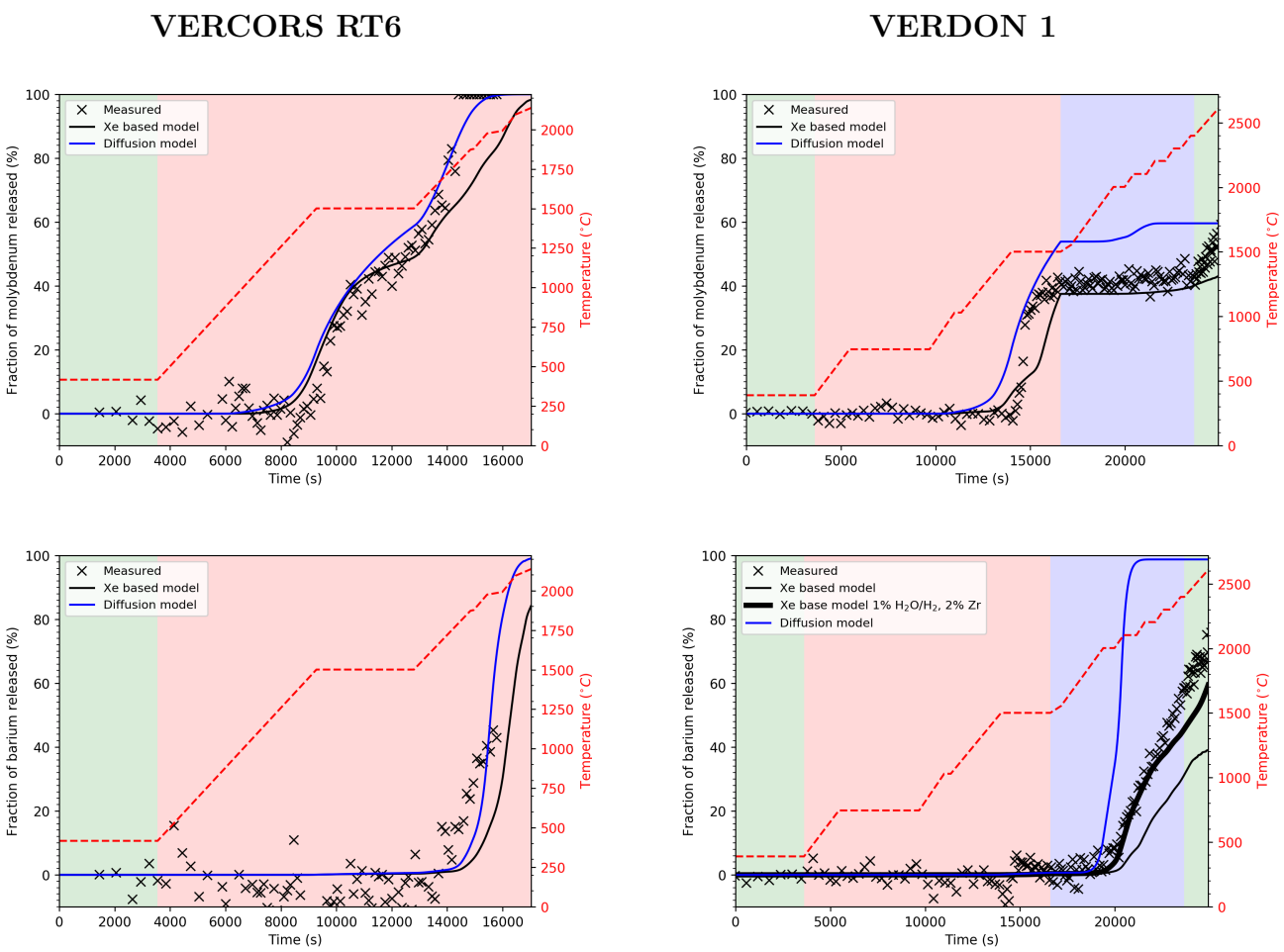

Figure 11: Calculated and measured fractions of molybdenum (top) and barium (bottom) released during the RT6 (left) and VERDON 1 (right) tests.

The chemical speciation of molybdenum in condensed and gas phases during the RT6 and the VERDON 1 tests are given in Figure 12 as a function of temperature.

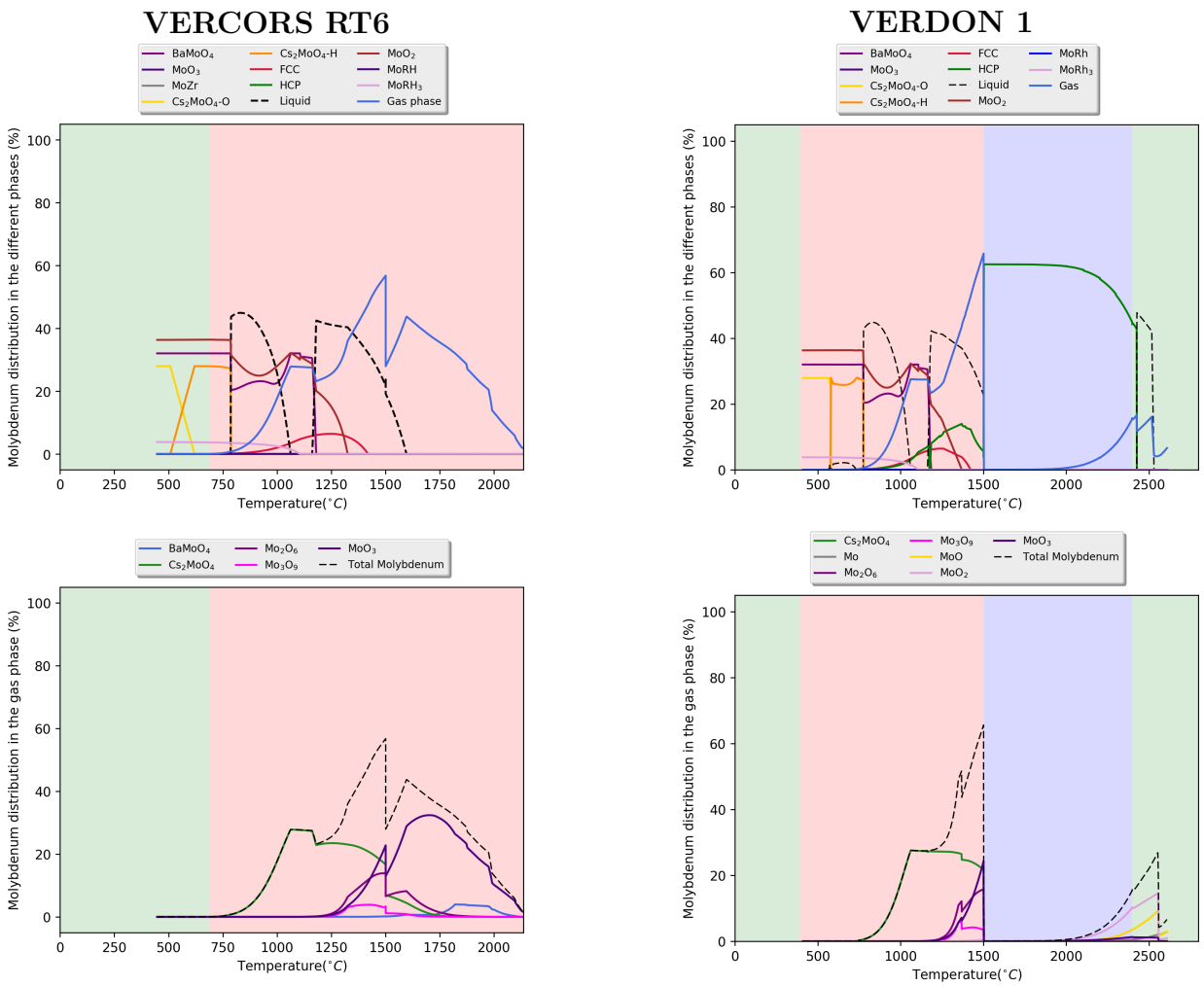

Figure 12: Calculated chemical speciation of molybdenum in the condensed (top) and gas (bottom) phases during the RT6 (left) and VERDON 1 (right) tests as a function of temperature. Calculations made with the Xe based model.

As can be seen, the speciation of Mo in the condensed phases is very complex since it is associated with Ba ($BaMoO_4$), Cs (Cs_2MoO_4-H and Cs_2MoO_4-O), and Ru, Rh, Tc and Pd in the FCC and HCP metallic phases. The speciation in the gas phase is simpler. During stage 2 of both tests, gaseous Mo (in Cs_2MoO_4) appears at a temperature slightly above 750 °C following the formation of a liquid phase (due to the solid-liquid transition of Cs_2MoO_4-H, which dissolves part of the Ba of the fuel) that progressively vaporizes at higher temperature. The agreement between the calculated and measured fractions of molybdenum released during stage 2 is associated with the formation of molybdenum oxides (MoO_3, Mo_2O_6, Mo_3O_9, MoO_2, MoO in decreasing order of proportion) in non negligible quantities above 1300 °C. These oxides increase the quantity of molybdenum in the gas phase up to 70 %.

In fact, parametric studies not shown here indicate that the formation or not of the gaseous molybdenum oxides depends mostly on the total gas content of the carrier gas in the calcula-

tions. Presently, their formation is a pure consequence of the unrealistic gas content considered by Geiger et al. [7]. In the coupled simulations presented by Germain et al. [15] where a realistic total gas content was considered, cesium dimolybdate compounds have been introduced in the thermodynamic database (TBASE), as suggested in a previous study by Riglet-Martial et al. [32], using the thermodynamic data recently published in reference [33]. As expected, the simulation results showed that the $Cs_2Mo_2O_7$ gaseous species is strongly stabilized, to the detriment of Cs_2MoO_4, when realistic experimental conditions are considered, which contribute to significantly enhance the Mo content in the gas phase, though Mo oxides gaseous species are actually found in minor amount. Then, updating the database with compounds of importance in the actual test conditions has led to excellent agreement with the Mo released fraction curves. As of today, similar calculations cannot be carried out with the TAF-ID V8 since the cesium polymolybdate compounds are not included in the database.

During stage 3 of the RT6 test, the Mo chemical speciation in the gas phase is conserved but the proportion of MoO_3 increases with temperature until the release rate exceeds the formation rate. The reducing conditions during stage 3 of the VERDON 1 test lead to the precipitation of all remaining Mo in metallic form (HCP), of low volatility versus temperature. This explains the lack of release of Mo during the first part of stage 3 and its moderate release from 2000 °C and beyond (less than 25 % of the total Mo is in the gas phase at the end of stage 4, in spite of changing the atmosphere from H_2 to He between stage 3 and 4).

The chemical speciation of barium in condensed and gas phases during the RT6 and the VERDON 1 tests are given in Figure 13 as a function of temperature. As shown in Figure 13, barium is not available in the gas phase during stage 2 of the RT6 and VERDON 1 tests due to the low volatility of $BaMoO_4$ or $BaZrO_3$ at temperatures less than 1500 °C. It is mostly found in solid $BaMoO_4$ until the solid-liquid phase transition that takes place close to 1200 °C. Ba is then progressively dissolved in tetragonal ZrO_2 (ZrO_2-T) with the disappearance of the liquid phase. Continuity holds at the interface between stage 2 and 3 of the RT6 test where 100 % of the Ba is found dissolved in tetragonal ZrO_2 (ZrO_2-T) at 1750 °C. Vaporization of part of the Ba occurs above 1780 °C leading to gaseous $BaMoO_4$ and BaO. The percentage of Ba in the gas phase reaches a maximum of almost 50 % at 2000 °C. It then progressively decreases with the gas release from the fuel. Above 1780 °C, the non gaseous Ba is found in $BaZrO_3$ and dissolved in the fluorite $(U,Zr)O_2$ phase.

The discontinuous conditions between stages 2 and 3 during the VERDON 1 test with a drop in the oxygen chemical potential leads to the instantaneous incorporation of all the Ba in ZrO_2-T, a phenomenon that was progressive during RT6. At 1780 °C, vaporization of Ba takes place leading to gaseous Ba, BaO and BaOH. The reducing conditions that stabilize Mo under its metallic form prevent the formation of gaseous $BaMoO_4$. The proportion of Ba in the gas phase reaches a maximum of 75 % at 2100 °C. It then decreases with the gas release from the fuel. As for RT6, the non gaseous Ba is incorporated in $BaZrO_3$ and dissolved in the $(U,Zr)O_2$ phase. During stage 4, all Ba is gaseous with a speciation identical to stage 3.

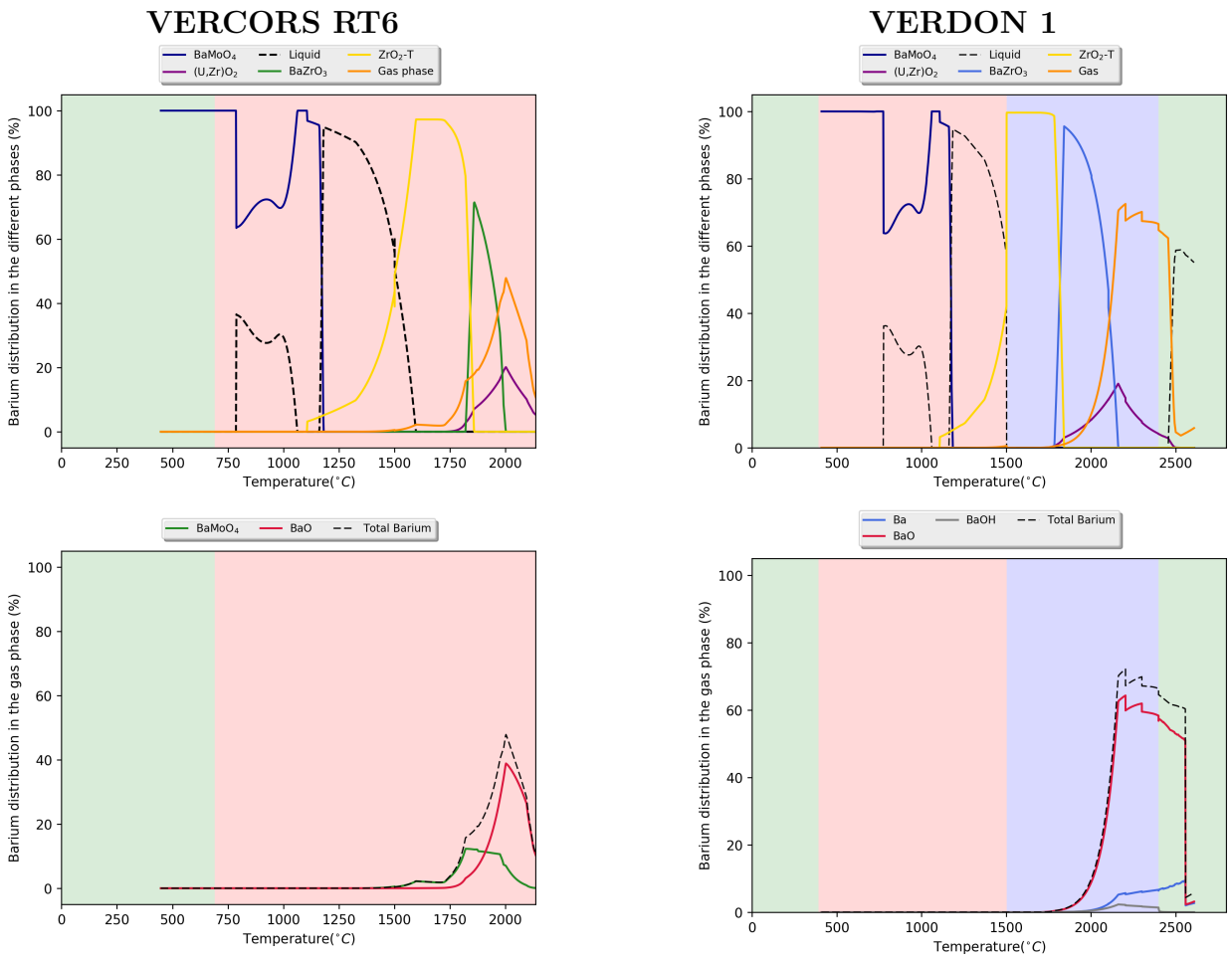

Figure 13: Calculated chemical speciation of barium in the condensed (top) and gas (bottom) phases during the RT6 (left) and VERDON 1 (right) tests as a function of temperature. Calculations made with the Xe based model.

As discussed in a previous paper by Germain et al. [15], the quantity of barium in the gas phase in reducing conditions is extremely sensitive to the residual amount of water vapor in the furnace (due to the formation of $BaH_2O_{2(g)}$) and to the clad Zr content considered in the calculations. Simulations of the VERCORS 4 test (reducing conditions, fuel with an average burnup of 40 GWd/tU) led to an excellent agreement with the measured Ba release if a 1 % residual H_2O content in the gas phase and 2 % of the Zr cladding in interaction with the fuel were considered during stage 3 in the calculation. Using the same conditions during stages 3 and 4 of the VERDON 1 simulation leads to a proportion of BaO in the gas phase that exceeds 80 % (instead of 60 % in the reference calculation) and consequently to a release rate that is in perfect agreement with on-line measurements, see Figure 11 where the thick black line indicates the new simulation result. Note that this small change in the carrier gas composition does not modify significantly the release of the other FPs, the speciation of which is independent of the H_2O content. The consideration of only 2 % of the Zr cladding instead of the total Zr cladding

content in the calculation of Geiger et al. [7] is also consistent with the sole interaction of the fuel periphery with the cladding, as observed after the VERDON 1 test [4].

3.4.5 Clad zirconium and other low-/non-volatile FPs

The chemical speciation of zirconium among phases during the RT6 and VERDON 1 tests are given in Figure 14 as a function of temperature.

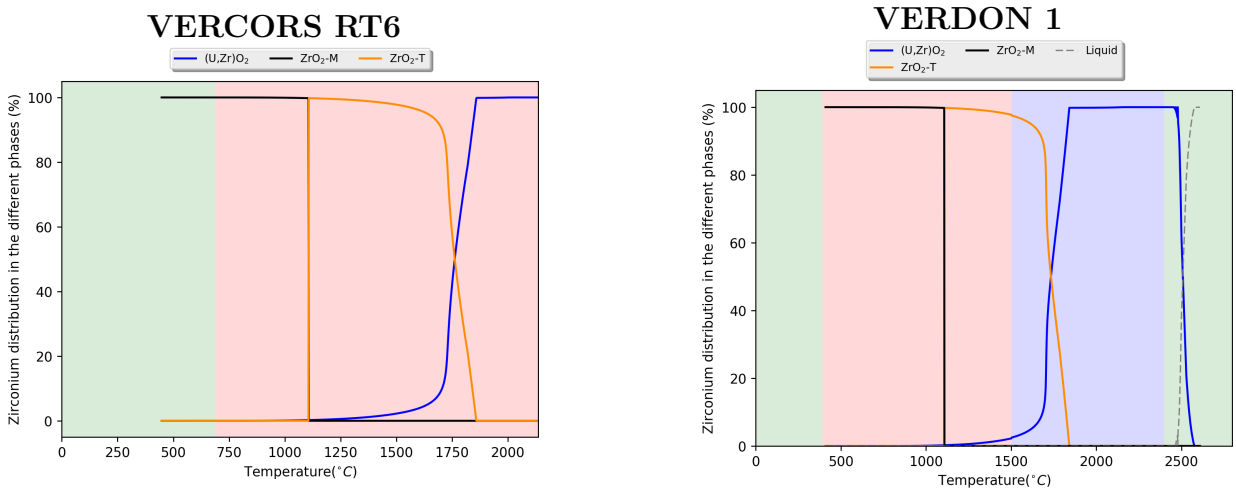

Figure 14: Chemical speciation of zirconium among phases during the RT6 (left) and VERDON 1 (right) tests as a function of temperature. Calculations made with the Xe based model.

The simulation results show that the chemical speciation of Zr during stages 2 and 3 is not dependent on the oxidizing or reducing conditions at hand. In fact, it is known from experiments (on-line measurements of H_2 release) that full oxidation of the Zr cladding occurs during stage 1, at temperatures lower than 1000 °C. During stage 2, a phase transition from monoclinic to tetragonal ZrO_2 takes place at 1100 °C. This leads to the dissolution of Zr (up to 6 %) in the (U,Zr)O_2 fluorite phase. At around 1675 °C, a miscibility gap appears and a second (U,Zr)O_2 fluorite phase is formed (not distinguished from the first one in Figure 14 but characterized by the change of slope of the blue curves) that progressively gather all the Zr available with temperature increase. At 1850 °C, all the U from the fuel is also found in the (U,Zr)O_2 phase. During RT6, the moderate maximum temperature of 2300 °C does not lead to the melting of the (U,Zr)O_2 phase, in contradiction with the observations reported during the test. The higher temperature range during the VERDON 1 test leads to the melting of the phase between 2500 and 2600 °C, as reported by Geiger et al. [7] and confirmed by post-test observations [4].

The calculated Released Fractions (RF) of a selection of FPs at the end of the simulations are compared in Figure 15 to measurements performed during the test (on-line) or after the tests (residual content divided by initial content). Calculated data regarding uranium and plutonium are also indicated in the Figure. Note that the measured and calculated values for

RT6 are those recorded at the beginning of melting during the test (2100 °C) since further measurements were not possible due to fuel "collapse".

As can be seen in Figure 15, there is a general agreement between calculated and measured RFs. The best match is obtained for the RT6 test with the Xe based model. The diffusion model gives systematically conservative estimates of the FPs final release. For the VERDON 1 test, the conclusion is less clear but it must be recalled that the release kinetics of most of the FPs are not well predicted with the diffusion model (see Figures 7, 9 and 11). Among the low volatile FPs, only La and to a lesser extent Ce releases seem respectively overestimated/ underestimated by the coupled simulation. La speciation indicates the formation of gaseous LaO during stages 3 and 4 of the tests leading to non-negligible releases. A Ce oxide appears during stage 4 of the VERDON 1 test, which explains the 9 % release in reducing conditions. Ru oxidation at high temperature is well captured by the simulation leading to 23 % release during RT6 and 6 % during VERDON 1, in consistency with the measured 28.1 and 1.3 %. Note that another measurement for Ru (5 %) closer to the estimated 6 % is available from the quantity deposited in the VERDON testing device.

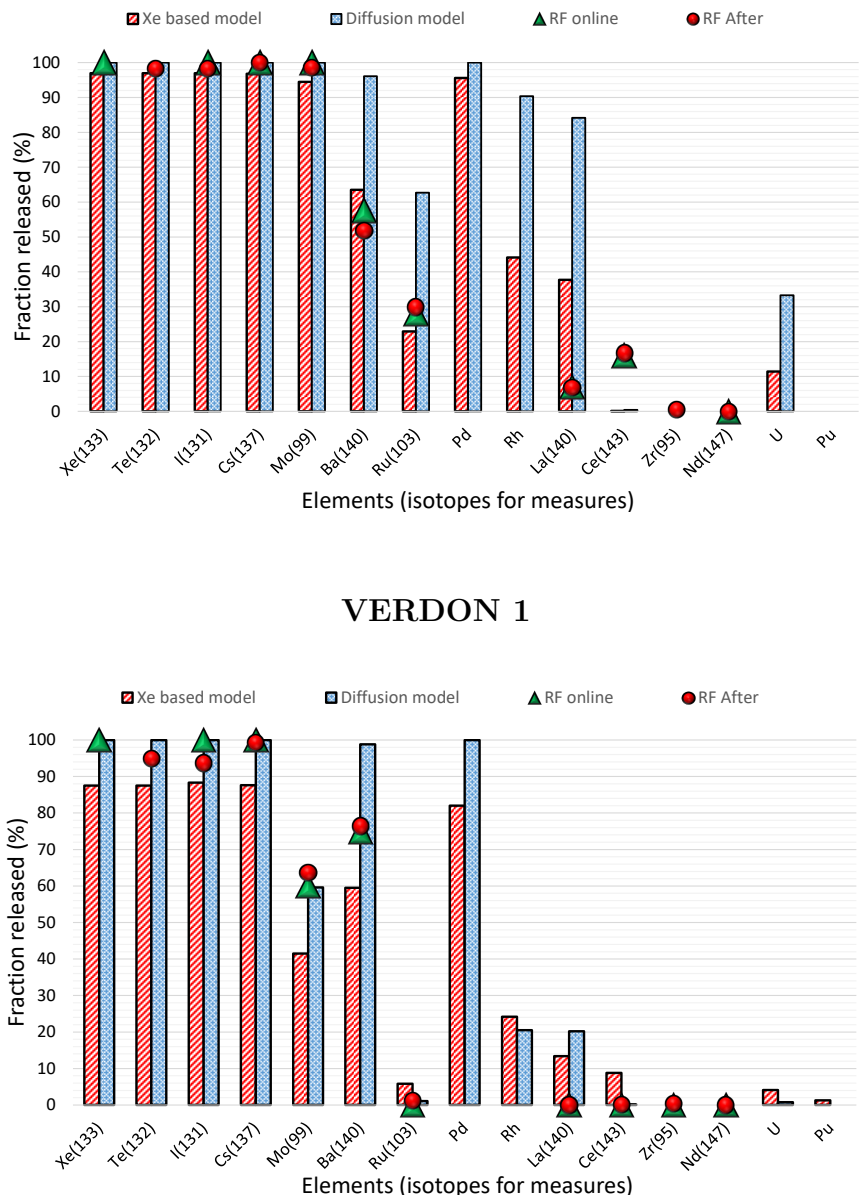

Figure 15: Calculated Released Fractions (RF) of the FPs during the RT6 (left) and VERDON 1 (right) tests compared to online and post-test measurements (RT6 data from [24], VERDON 1 data from [1]).

The totally non volatile FPs include here Nd and Zr. Gaseous uranium trioxide is also formed at the end of stage 3 and during stage 4 (temperature above 2200 °C). This leads to

an 11.4 % / 4.1 % RF at the end of RT6/ VERDON 1 tests (not measured after these tests). Plutonium RF (not measured) is on the contrary null, except during the very high temperature stage of the VERDON 1 test (1.3 %).

4 Discussion

The first objective of this paper was to test the validity of a thermochemical - gas diffusion coupling where the gas transport model does not differentiate the FPs but considers the gas phase as a single entity transported outside of the fuel as a whole. The relevant key points of the model is that the differentiation of chemically reactive FPs release depends heavily on the quality of the thermodynamic data, on the representativity of the initial FPs content and test conditions and on the modeling of the U-O-FPs system. The advantage is that a rather simple model for gas transport with only two parameters can be used, provided it fits well with the release rate of a FP available in high quantity in the fuel and non-chemically reactive with the other FPs. In this work, Xe has been selected for that purpose. A model describing gas diffusion within a spherical fuel grain and instantaneous release at the grain boundary has been implemented and fitted on the measured Xe release rate. A specificity is the inclusion in the diffusion equation of the gas species formed from the chemically reactive FPs (term $\partial S_{FP}/\partial t$ in equation 1). To analyze the impact of any error in the modeling of Xe diffusion, the measured Xe release rate has also been used directly in the coupled simulations.

The agreement between the calculated release curves for the I, Te and Cs volatile FPs and the measurements is not surprising considering their 100 % availability at low temperatures in the gas phase. Cesium is used in some severe accident codes as a reference for fitting the release rate with a gas diffusion model similar to the one considered in this work [14]. Cesium release kinetics are sensitive to the fuel burnup, which explains its use for gas release fitting. The RF curves of the semi-volatile Mo and Ba are very well reproduced by the simulation based on the measured Xe release rate, demonstrating the sensitivity to oxidizing/reducing conditions. Significant Pd RFs were calculated, consistent with Mo RFs and more important in oxidizing conditions as was expected from measures performed after some of the VERCORS tests [25]: RFs of 15 % and 45 % were measured after the RT3 (reducing conditions) and RT4 (oxidizing conditions) tests performed on a UO_2 fuel sample with a burnup of 38-39 GWd/tU. Significant RFs of the low volatile Ru were obtained in the simulations but with a much higher RF in oxidizing conditions. These results are also in good agreement with the VERCORS test results [25]. The calculated Ce RFs indicate a higher release during the VERDON 1 reducing conditions, as was expected from the past VERCORS tests. The 16 % RF of Ce measured after the RT6 test is the sole exception in the VERCORS database with respect to this trend. It is clearly not reproduced by the simulation. La is also generally expected to be more sensitive to reducing conditions, with RFs below 10 %. The comparison of the measured La RFs after the RT6 and VERDON 1 tests show the opposite trend (6 % after RT6, 0 % after VERDON 1). The simulations give the same tendency (higher RF in oxidizing conditions) but with RFs greatly overestimated (38 % after RT6 and 13 % after VERDON 1). Non volatile FPs (e.g., Zr and Nd) are, as expected from their classification, not released during the simulations. A non-

negligible proportion of U is predicted to be released from the fuel during the RT6 simulation (11 %), favored by the formation of U gaseous oxides. The calculated RF is lower during the VERDON 1 test (4 %). This trend and the magnitude of the RFs are in good agreement with the measurements by Inductively Coupled Plasma Mass Spectrometry (ICP-MS) during other VERCORS tests (between 1 and 10 % [25]). Chemical analyses of Pu after the RT test series led to estimated RFs less than 1 % which agree well with the calculated 1.3 % during the very high temperature sequence of the VERDON 1 test.

These results tend to validate the proposed coupling between fission gas release and irradiated fuel thermochemistry. It shows that a gas transport mechanism identical for all the gases in the fuel and consistent with the behavior of the bulk of the gas phase consisting of the chemically non-reactive noble gases, can lead to a differentiation of the FPs RFs and release rates provided the U-O-FPs thermochemistry is well assessed. It must be stressed again that the thermochemical description of the U-O-FP system at hand is related to the initial test conditions considered (strong overestimation of the gas phase in the present case leading to unrealistic conditions).

The improvement of the TAF-ID on this point, in order to obtain a consistent thermochemical modeling under realistic test conditions, was out of scope of the present paper. Nevertheless, these results represent a first step towards the potential treatment of severe accident tests in fuel performance codes since the proposed coupling is not restricted to the two parameters diffusion model considered in this work. The definition of the instantaneous fission gas release of equation 4 could easily be based on the mechanistic models already implemented in many fuel performance codes [34][35][36][37] that provide a much more detailed description of fission gas distribution (within bubbles in the grains or at the grain boundaries, dissolved in the grains ...).

One interesting outcome of these models with respect to severe accidents tests is the potential differentiation of inter- and intra-granular gas release, as shown for instance by the comparison of the ^{133}Xe and ^{85}Kr release rates during some of the VERCORS tests [38] (the long life ^{85}Kr isotope includes the inter-granular gas inventory that has accumulated during the nominal irradiation). However, two main difficulties remain. First, the distribution of FPs in the gas bubbles (within the grain or at the grain boundaries) will need to be defined. Separate thermochemical equilibrium calculations relative to both gas bubble population could be performed. The second difficulty concerns the modeling of gas bubble migration in severe accident test sequences where uniform temperature conditions generally prevail. In most mechanistic gas models, bubble transport in the grain is dependent on the sole temperature gradient in the fuel. In the MFPR code, which describes the fission products distribution and migration mechanisms within an elementary representative fuel grain (and boundaries), a specific bubble transport mechanism associated to dislocations ensures a proper modeling of the release of the FPs trapped in gas bubbles [12][11][39]. Introduction of sophisticated thermo-mechanics (clad failure [40], fuel fragmentation [41]) in the modeling of severe accident tests is also one of the potential outcome of simulations with fuel performance codes. They could have consequences on FPs release rates as inferred by the FPs release bursts observed after clad failure in some of the VERCORS/VERDON tests.

The second point of discussion concerns the differences in fuel “collapse” temperatures

between the RT6 and VERDON 1 tests. Fuel "collapse" started at 2100 °C during the RT6 test and was complete at 2200 °C. The fuel did not collapse during the VERDON 1 test in spite of the much higher temperature recorded (2610 °C). Signs of fuel-clad local melting were however observed after the VERDON 1 test [4] showing that the fuel collapse was probably imminent. In both cases and in particular for RT6, the collapse temperature is far below the expected solidus temperature of a non-irradiated stoichiometric fuel (2874 °C) or of an irradiated fuel up to 72 GWd/tU (2838 °C [42]). As discussed by Pontillon et al. [43], the VERCORS tests series HT had already pointed out the role of oxidizing conditions in the lowering of the fuel collapse temperature. The comparison of the RT6 and VERDON 1 tests confirmed this trend [1] and excluded definitively a burnup effect.

The comparison of the fuel collapse temperatures during the RT3 (2700 °C) and RT4 (2250 °C) tests performed on UO_2 fuel debris respectively without and with Zr showed furthermore the importance of ZrO_2 in the lowering of the melting temperature. Considering the long oxidizing plateau at 1500 °C during most of the VERCORS tests, it seems unrealistic to expect the presence of non-oxidized Zr in contact with the fuel at high temperatures. Melting of UO_2-ZrO_2 is usually associated with the formation of a eutectic at 2530 °C, which is much higher than the "collapse" temperature in RT6 (2200 °C). Based on the experimental work of Manara [3], Barrachin et al. attributed the low "collapse" temperature to the strong dependency of the solidus temperature (and to a lesser extent the liquidus temperature) on the stoichiometry deviation of UO_{2+x} [5]. They assumed that the fuel could be strongly oxidized before it would be dissolved in the oxidized cladding. Their reassessment of the U-O and U-Zr phase diagrams with Manara's measures led to the calculation of solidus/liquidus temperatures in mixed oxides systems $(U,Zr)O_{2+x}$ that decreased with the stoichiometry deviation [5]. For $x \sim 0.1$, the calculated solidus temperature was found to be close to the "collapse" temperature of the RT6 test (2200 °C).

The models behind the description of the U-O system in the TAF-ID include the solidus and liquidus temperatures measured by Manara et al. [3]. The original U-O model developed by Gueneau et al. [44] was reassessed in 2011 to account for these measurements [27]. The U-O phase diagram in the stoichiometric region of interest is plotted in Figure 16.

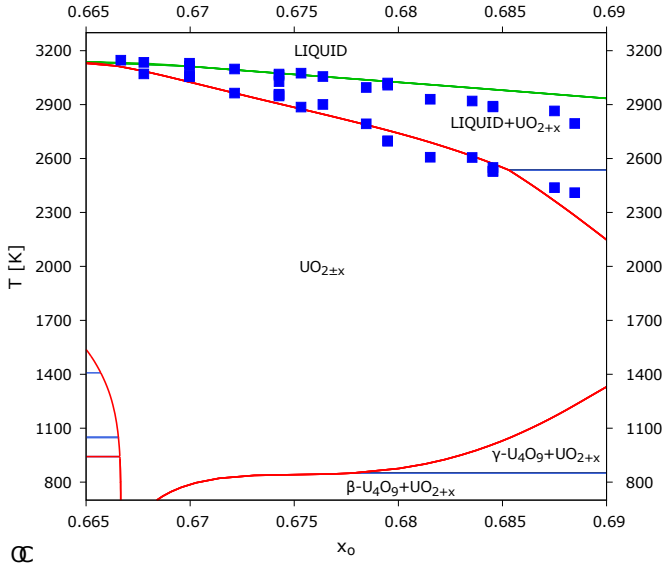

Figure 16: U-O phase diagram as calculated with the TAF-ID and OC and experimental measurements of solidus and liquidus temperatures (blue squares) by Manara et al. [3]

The data by Manara et al. are reported on the Figure and match the solidus and liquidus lines [3]. The data of Manara et al. were furthemore obtained at very high pressure to suppress the gas phase. Barrachin et al. showed that shifting the pressure from 1 to 2 bars led to a decrease of the melting temperature of the (U,Zr)O_{2+x} phase of 100 °C [5]. It was also proposed by Barrachin et al. [5] that the contact between the cladding and the fuel plays a role in lowering the melting temperature. It was shown that the contact is greater in oxidizing atmosphere compared to reducing atmosphere, which could partially explain the difference in melting temperatures.

The UO_2-ZrO_2 phase diagram from the TAF-ID reproduced in Figure 17 shows the formation and melting of a UO_2-ZrO_2 eutectic at a temperature around 2500 °C, as expected from the known behavior of the system. The U-O, U-Zr and U-Zr-O systems included in the TAF-ID have been described by Quaini et al. [45] with numerous comparisons to experimental measurements. It must be pointed out that most of the selected experimental data concern the UO_2-Zr or UO_2-α-Zr sections between 1730 and 2330 °C due to the particular interest on corium behavior where a significant part of non oxidized cladding remains.

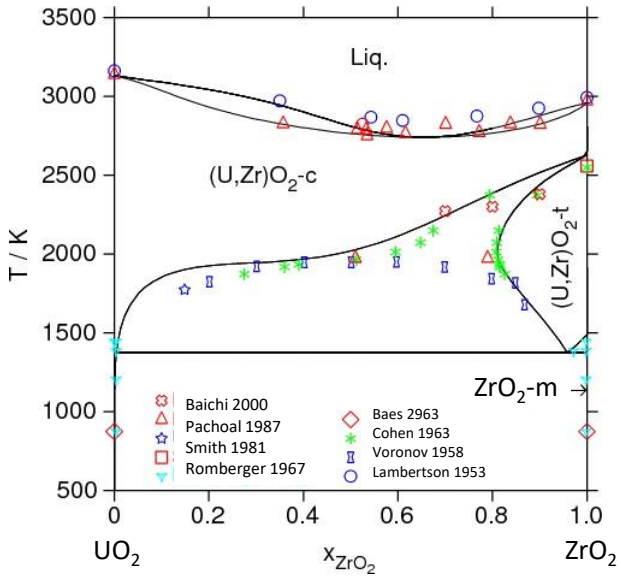

Figure 17: UO_2-ZrO_2 phase diagram as calculated with the TAF-ID and TC (reproduced from [45]).

In the VERDON 1 simulation, melting of a quasi-stoichiometric (U,Zr,FP)O_2 phase was obtained at a temperature between 2500 °C (beginning) and 2600 °C (full melting), in agreement with the thermochemical calculations of Geiger et al. [7]. No melting was predicted in the simulation of the RT6 test. In order to take into account a potential uncertainty in the recorded temperature, the fuel composition (U-O-Zr and remaining FPs) in the RT6 test obtained at 2200 °C has been considered in independent thermochemical calculations with OC and the TAF-ID where only temperature was increased. Melting of a quasi-stoichiometric (U,Zr)O_2 phase was found to start at 2470 °C and end at 2530 °C, that is to say at a temperature 70 °C lower than during the VERDON 1 test. The difference is related to the smaller O/(Zr+U) ratio of the liquid phase formed in the VERDON 1 test (2.01) compared to RT6 (2.017). The impact of the oxygen and zirconium contents on the (U,Zr)$O_{2\pm x}$ phase at 2230 °C is illustrated in Figure 18, obtained from independent calculations with the TAF-ID and TC. The RT6 calculation result is also indicated in the figure.

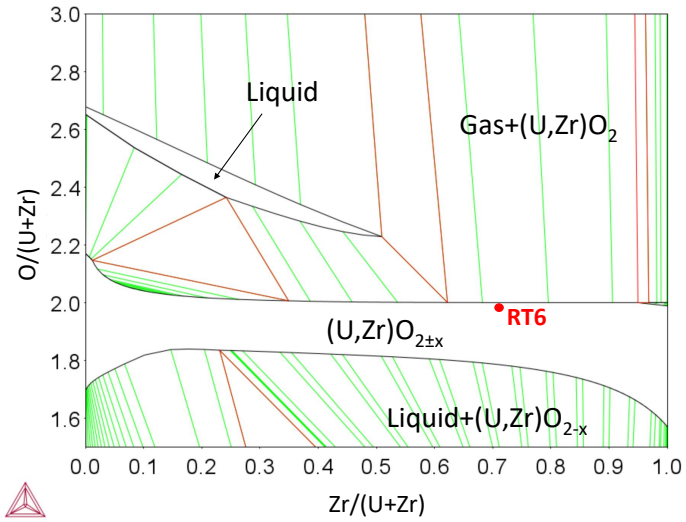

Figure 18: $(U,Zr)O_{2\pm x}$ phase diagram calculated at 2230 °C with the TAF-ID showing the RT6 calculation result at the same temperature

Figure 18 shows that solid-gas or solid-liquid transitions at 2230 °C are likely in case of a small hyperstoichiometry of the $(U,Zr)O_{2+x}$ phase. During RT6, an important quantity of gaseous UO_3 is predicted to form at temperatures above 2000 °C. The associated release of O during the high temperature part of the tests is at the origin of the limited hyperstoichiometry of the phase. Note that an over-estimation of the uranium trioxide gas release during the test due to unrealistic test conditions considered in the calculation (great overestimation of the gas phase) cannot be excluded, which could explain the limited hyperstoichiometry of the final fuel material. According to Figure 18, in case the U-Zr-O solution contains less Zr ($Zr/(U+Zr) < 0.6$), a solid-liquid transition is likely at 2230 °C. The consideration of all the clad Zr and the assumption of a perfect blend with the fuel in the calculations is therefore another potential reason for the overestimated melting temperature.

It must be furthermore pointed out that the composition of the quasi-stoichiometric $(U,Zr)O_2$ phase calculated by Geiger et al. [7] in the VERDON 1 test was far from the measured composition of two of the three distinct $(U,Zr)O_{2-x}$ phases identified at the periphery of the VERDON 1 fuel sample after the test [4]. The microstructure in this region was highly heterogeneous and reflected the progressive penetration in the fuel cracks of a melted $(U,Zr)O_2$ phase carrying FPs from the pellet periphery. Diffusion of Zr in the fuel material in contact with the melt took place leading to a transition zone with a high Zr content. Unfortunately, similar measurements are not available for RT6 but it is highly possible that Zr or O diffusion mechanisms took place during the test leading to a melting of the UO_2-ZrO_2 material at a lower temperature than expected. In this respect, independent calculations with the TAF-ID and OC on the fuel composition (U-O-FPs) of the RT6 test obtained at 2200 °C were performed without the cladding leading an O/M ratio of 2.02, a solidus temperature of 2267 °C and a liquidus temperature of 2312 °C (the impact of FPs on the melting temperature is taken into account in the calculations but is small compared to that of the stoichiometry deviation of the fuel [6]). It is therefore

highly possible that the fuel center with no contact with the clad Zr melted first during the RT6 test. The periphery of the fuel in contact with ZrO_2 is also characterized by a much higher burnup than the rest of the pellet ($\geq$ 150 GWd/tU) and a build-up of Pu. In consequence, the inventory is different from the one used in the simulations which describes the average FPs content of the pellet. This might also induce some differences in the melting temperature of the fuel-clad mixture. A simulation of the VERDON/VERCORS test sequence with detailed burnup / FP radial profiles is necessary to study this potential rim effect.

5 Conclusions

In this paper, simulations of the VERDON 1 and RT6 tests on high burnup fuel considering a coupling between irradiated fuel thermochemistry and a fission gas release model have been detailed. The thermochemical calculations make use of the TAF-ID for the description of the phases likely to form from the 15 fission products considered in the fuel (Ba, Ce, Cs, I, La, Mo, Nd, Np, Pd, Rh, Ru, Sr, Tc, Te, Zr) and of the OpenCalphad thermochemical solver for the minimization of the Gibbs energy of the system. The gas release model describes the diffusion of the gases within an equivalent spherical grain and includes the contribution of gases formed by reaction between the FPs.

The coupled simulations led to a very good agreement with the release kinetics of various fission products (I, Te, Cs, Mo, Ba) in spite of the simplicity of the gas diffusion model where no distinction between the fission products is made. The differentiation of FPs release rates depends only on the FPs state (in solid, liquid or gas phase) in the fuel as obtained from the thermochemical calculations. The small releases of the low volatile FPs are also correctly assessed, for most of them. These results show the crucial importance of the thermodynamic representation of the U-O-FPs system. In this work, for sake of comparison, the metholology proposed by Geiger et al. [7] was used as it is in spite of the unrealistic initial conditions used (great overestimation of the gas phase) as compared to the actual test conditions. Complementary work has to be done on this aspect to update the database with some relevant compounds likely to form in the specific VERCORS and VERDON test conditions. The introduction of cesium polymolybdate compounds could help to address this issue, as discussed in references [15] and [32].

The fuel "collapse" at low temperature related to the melting of a (U,Zr)O_{2+x} phase was also investigated but could not be obtained in the test conditions of the RT6 test performed in oxidizing conditions. The description of the U-O-Zr system available in the TAF-ID, discussed in the paper, is not at the origin of this result. As shown by the (U,Zr)O_{2+x} phase diagram, the fuel collapse at low temperature could be explained by the interaction between UO_{2+x} and Zr wich could lead to the formation of a liquid phase (U,Zr)O_{2+x} at around 2190 °C or by the lower melting temperature of the oxidized irradiated fuel alone (2267 °C) that may initiate at the pellet center. In any case, a more precise description of the fuel (radial discretization) and of the fuel-clad interaction at the pellet periphery only with the consideration of the locally much higher burnup could potentially improve the simulation results.

Acknowledgements

The CEA authors would like to acknowledge EDF and FRAMATOME for their technical and financial support to this work. Special thanks are adressed to Ernesto Geiger, Faculty of Energy Systems and Nuclear Science, Ontario Tech University, Canada, for fruitful discussions on his thermodynamic calculations. The reviewers are acknowledged for their careful reading and correction of the paper.

References

[1] Y. Pontillon, E. Geiger, C. Le Gall, S. Bernard, A. Gallais-During, P.P. Malgouyres, E. Hanus, and G. Ducros. Fission products and nuclear fuel behaviour under severe accident conditions. Part 1: main lessons learnt from the first VERDON test. *Journal of Nuclear Materials*, 495:363–384, 2017.

[2] G. Ducros, P.P. Malgouyres, M. Kissane, D. Boulaud, and M. Durin. Fission product release under severe accidental conditions: general presentation of the program and synthesis of VERCORS 1–6 results. *Nuclear Engineering and Design*, 208(2):191–203, 2001.

[3] D. Manara, C. Ronchi, M. Sheindlin, M. Lewis, and M. Brykin. Melting of stoichiometric and hyperstoichiometric uranium dioxide. *Journal of Nuclear Materials*, 342(1-3):148–163, 2005.

[4] E. Geiger, C. Le Gall, A. Gallais-During, Y. Pontillon, J. Lamontagne, E. Hanus, and G. Ducros. Fission products and nuclear fuel behaviour under severe accident conditions. Part 2: Fuel behaviour in the VERDON-1 sample. *Journal of Nuclear Materials*, 495:49–57, 2017.

[5] M. Barrachin, P.Y. Chevalier, B. Cheynet, and E. Fischer. New modelling of the U–O–Zr phase diagram in the hyper-stoichiometric region and consequences for the fuel rod liquefaction in oxidising conditions. *Journal of Nuclear Materials*, 375(3):397–409, 2008.

[6] C. Guéneau, N. Dupin, L. Kjellqvist, E. Geiger, M. Kurata, S. Gossé, E. Corcoran, A. Quaini, R. Hania, A.L. Smith, et al. TAF-ID: an international thermodynamic database for nuclear fuels applications. *Calphad*, 72:102212, 2021.

[7] E. Geiger, C. Guéneau, Y. Pontillon, and E.C. Corcoran. Modelling nuclear fuel behaviour with TAF-ID: Calculations on the VERDON-1 experiment, representative of a nuclear severe accident. *Journal of Nuclear Materials*, 522:294–310, 2019.

[8] M.H.A. Piro. Thermodynamically Informed Nuclear Fuel Codes—A Review and Perspectives. *Thermo*, 1(2):262–285, 2021.

[9] B.J. Lewis, B.J. Corse, W.T. Thompson, M.H. Kaye, F.C. Iglesias, P. Elder, R. Dickson, and Z. Liu. Low volatile fission-product release and fuel volatilization during severe reactor accident conditions. *Journal of Nuclear Materials*, 252(3):235–256, 1998.

[10] G. Brillant, C. Marchetto, and W. Plumecocq. Fission product release from nuclear fuel. I. physical modelling in the ASTEC code. *Annals of Nuclear Energy*, 61:88 – 95, 2013.

[11] M.S. Veshchunov, V.D. Ozrin, V.E. Shestak, V.I. Tarasov, R. Dubourg, and G. Nicaise. Development of the mechanistic code MFPR for modelling fission-product release from irradiated UO_2 fuel. *Nuclear Engineering and Design*, 236(2):179–200, 2006.

[12] M.S. Veshchunov, R. Dubourg, V.D. Ozrin, V.E. Shestak, and V.I. Tarasov. Mechanistic modelling of urania fuel evolution and fission product migration during irradiation and heating. *Journal of Nuclear Materials*, 362(2):327–335, 2007.

[13] D.R. Olander and V. Mubayi. Review of the materials-chemistry models in the VICTORIA code. *Journal of Nuclear Materials*, 270(1-2):1–10, 1999.

[14] R.O. Gauntt. MELCOR 1.8.5 Modeling aspect of fission product release, transport and deposition. Technical report, 1635, Sandia National laboratory, Albuquerque, USA, 2010.

[15] A. Germain, J. Sercombe, C. Riglet-Martial, C. Introini, L. Noirot, Y. Pontillon, and P. Maugis. Coupled modeling of irradiated fuel thermochemistry and gas diffusion during severe accidents. *Accepted in the Journal of Nuclear Materials*, November 2021.

[16] J. Sercombe, B. Michel, and C. Riglet-Martial. 2.14 - Modelling of pellet cladding interaction. In R.J.M. Konings and R.E. Stoller, editors, *Comprehensive Nuclear Materials*. Elsevier, Oxford, 2020.

[17] B. Michel, C. Nonon, J. Sercombe, F. Michel, and V. Marelle. Simulation of pellet-cladding interaction with the PLEIADES fuel performance software environment. *Nuclear Technology*, 182(2):124–137, 2013.

[18] B. Sundman, U.R. Kattner, M. Palumbo, and S.G. Fries. OpenCalphad - a free thermodynamic software. *Integrating Materials and Manufacturing Innovation*, 4(1):1, 2015.

[19] B. Sundman, U.R. Kattner, C. Sigli, M. Stratmann, R. Le Tellier, M. Palumbo, and S.G. Fries. The OpenCalphad thermodynamic software interface. *Computational Materials Science*, 125:188 – 196, 2016.

[20] C. Introïni, J. Sercombe, and B. Sundman. Development of a robust, accurate and efficient coupling between PLEIADES/ALCYONE 2.1 fuel performance code and the OpenCalphad thermo-chemical solver. *Nuclear Engineering and Design*, 369, 2020.

[21] C. Le Gall, E. Geiger, A. Gallais-During, Y. Pontillon, J. Lamontagne, E. Hanus, and G. Ducros. Fission products and nuclear fuel behaviour under severe accident conditions. Part 3: speciation of fission products in the VERDON-1 sample. *Journal of Nuclear Materials*, 495:291–298, 2017.

[22] A. Gallais-During, S. Bernard, B. Gleizes, Y. Pontillon, J. Bonnin, P.-P. Malgouyres, S. Morin, E. Hanus, and G. Ducros. Overview of the VERDON-ISTP program and main insights from the VERDON-2 air ingress test. *Annals of Nuclear Energy*, 101:109–117, 2017.

[23] Y. Pontillon, G. Ducros, and P.P. Malgouyres. Behaviour of fission products under severe PWR accident conditions: the VERCORS experimental program — Part 1: General description of the program. *Nuclear Engineering and Design*, 240(7):1843–1852, 2010.

[24] Y. Pontillon, G. Ducros, and P.P. Malgouyres. Behaviour of fission products under severe PWR accident conditions: The VERCORS experimental program — Part 2: Release and transport of fission gases and volatile fission products. *Nuclear Engineering and Design*, 240(7):1853–1866, 2010.

[25] Y. Pontillon, G. Ducros, and P.P. Malgouyres. Behaviour of fission products under severe PWR accident conditions. the VERCORS experimental program — Part 3: Release of low-volatile fission products and actinides. *Nuclear Engineering and Design*, 240(7):1867–1881, 2010.

[26] A. Gallais-During, J. Bonnin, P.-P. Malgouyres, S. Morin, S. Bernard, B. Gleizes, Y. Pontillon, E. Hanus, and G. Ducros. Performance and first results of fission product release and transport provided by the VERDON facility. *Nuclear Engineering and Design*, 277:117–123, 2014.

[27] C. Guéneau, N. Dupin, B. Sundman, C. Martial, J.-C. Dumas, S. Gossé, S. Chatain, F. De Bruycker, D. Manara, and R.J.M. Konings. Thermodynamic modelling of advanced oxide and carbide nuclear fuels: description of the U–Pu–O–C systems. *Journal of Nuclear Materials*, 419(1-3):145–167, 2011.

[28] B. Sundman. Modification of the two-sublattice model for liquids. *Calphad*, 15(2):109–119, 1991.

[29] J. Vidal, J. Groullier, A. Launay, Y. Berthion, S.A. Marc, and H. Toubon. CESAR: a code for nuclear fuel and waste characterisation. In *International Symposium Waste Management*, Tucson, Arizona, USA, 2006.

[30] A.H. Booth. A method of calculating fission gas diffusion from UO_2 fuel and its application to the X-2-f loop test. Technical report, 496, Atomic Energy of Canada Limited, Chalk River, Canada, 1957.

[31] M.H.A. Piro, M.J. Welland, and M. Stan. On the interpretation of chemical potentials computed from equilibrium thermodynamic codes. *Journal of Nuclear Materials*, 464:48 – 52, 2015.

[32] Ch. Riglet-Martial, J. Sercombe, and Y. Pontillon. Speciation and release kinetics of the fission products Mo, Cs, Ba and I from nuclear fuels in severe accident conditions. In *Topfuel conference*, Prague, Czech Republic, 2018.

[33] A.L. Smith, J. Vlieland, M.-C. Pignié, M. Abbink, G. Mikaelian, and P. Benigni. New insights into the Cs-Mo-O system: Experimental studies of the Cs_2MoO_4-MoO_3 pseudo-binary system. *Thermochimica Acta*, 696:178825, February 2021.

[34] L. Noirot. MARGARET: A comprehensive code for the description of fission gas behavior. *Nuclear Engineering and Design*, 241(6):2099–2118, 2011.

[35] G. Jomard, C. Struzik, A. Boulore, P. Mailhé, V. Auret, and R. Largenton. CARACAS, an industrial model for the description of fission gas behavior in LWR-UO_2 fuel. In *WRFPM conference*, Sendai, Japan, 2014.

[36] G. Khvostov, K. Mikityuk, and M.A. Zimmermann. A model for fission gas release and gaseous swelling of the uranium dioxide fuel coupled with the FALCON code. *Nuclear Engineering and Design*, 241(8):2983–3007, 2011.

[37] G. Pastore, L. Luzzi, V. Di Marcello, and P. Van Uffelen. Physics-based modelling of fission gas swelling and release in UO_2 applied to integral fuel rod analysis. *Nuclear Engineering and Design*, 256:75–86, 2013.

[38] Y. Pontillon, I. Moysan, S. Bernard, and M. Ledieu. New insight on volatile fission products (I and Cs) release from high burnup UO_2 fuel under LOCA type conditions. In *Topfuel conference*, Prague, Czech Republic, 2018.

[39] L. Verma. *Spatialized study of the coupling between extended defects and mobile species in the nuclear fuel*. PhD thesis, Aix-Marseille University, France, 2019.

[40] J. Sercombe, T. Helfer, E. Federici, D. Leboulch, T. Le Jolu, A.H. De Ménibus, and C. Bernaudat. 2D simulation of hydride blister cracking during a RIA transient with the fuel code ALCYONE. *EPJ Nuclear Sciences & Technologies*, 2:22, 2016.

[41] B. Michel, J. Sercombe, G. Thouvenin, and R. Chatelet. 3D fuel cracking modelling in pellet cladding mechanical interaction. *Engineering Fracture Mechanics*, 75(11):3581–3598, 2008.

[42] J.J. Carbajo, G.L. Yoder, S.G. Popov, and V.K. Ivanov. A review of the thermophysical properties of MOX and UO_2 fuels. *Journal of Nuclear Materials*, 299(3):181–198, 2001.

[43] Y. Pontillon, P.P. Malgouyres, G. Ducros, G. Nicaise, R. Dubourg, M. Kissane, and M. Baichi. Lessons learnt from VERCORS tests.: Study of the active role played by UO_2–ZrO_2–FP interactions on irradiated fuel collapse temperature. *Journal of Nuclear Materials*, 344(1):265–273, 2005.

[44] C. Guéneau, M. Baichi, D. Labroche, C. Chatillon, and B. Sundman. Thermodynamic assessment of the uranium–oxygen system. *Journal of Nuclear Materials*, 304(2):161–175, 2002.

[45] A. Quaini, C. Guéneau, S. Gossé, N. Dupin, B. Sundman, E. Brackx, R. Domenger, M. Kurata, and F. Hodaj. Contribution to the thermodynamic description of the corium–the U-Zr-O system. *Journal of Nuclear Materials*, 501:104–131, 2018.